Redox Biology 51 (2022) 102251

Contents lists available at ScienceDirect

Redox Biology

journal homepage: www.elsevier.com/locate/redox

Interplay between mitochondrial reactive oxygen species, oxidative stress and hypoxic adaptation in facioscapulohumeral muscular dystrophy: Metabolic stress as potential therapeutic target

Philipp Heher [a,*], Massimo Ganassi [a], Adelheid Weidinger [b,c], Elise N. Engquist [a], Johanna Pruller [a], Thuy Hang Nguyen [d], Alexandra Tassin [d], Anne-Emilie Declèves [e], Kamel Mamchaoui [f], Christopher R.S. Banerji [a], Johannes Grillari [b,c,g], Andrey V. Kozlov [b,c], Peter S. Zammit [a,**]

[a] Randall Centre for Cell and Molecular Biophysics, King's College London, Guy's Campus, London, UK
[b] Ludwig Boltzmann Institute for Traumatology. The Research Center in Cooperation with AUVA, Vienna, Austria
[c] Austrian Cluster for Tissue Regeneration, Vienna, Austria
[d] Laboratory of Respiratory Physiology, Pathophysiology and Rehabilitation, Research Institute for Health Sciences and Technology, University of Mons, 7000, Mons, Belgium
[e] Department of Metabolic and Molecular Biochemistry, Research Institute for Health Sciences and Technology, University of Mons, 7000, Mons, Belgium
[f] Institut de Myologie, Sorbonne University, INSERM UMRS974, Paris, France
[g] Institute for Molecular Biotechnology, University of Natural Resources and Life Sciences, Vienna, Austria

ARTICLE INFO

Keywords:
Facioscapulohumeral muscular dystrophy
DUX4
Reactive oxygen species
Mitochondrial dysfunction
Hypoxia
Antioxidants

ABSTRACT

Facioscapulohumeral muscular dystrophy (FSHD) is characterised by descending skeletal muscle weakness and wasting. FSHD is caused by mis-expression of the transcription factor DUX4, which is linked to oxidative stress, a condition especially detrimental to skeletal muscle with its high metabolic activity and energy demands. Oxidative damage characterises FSHD and recent work suggests metabolic dysfunction and perturbed hypoxia signalling as novel pathomechanisms. However, redox biology of FSHD remains poorly understood, and integrating the complex dynamics of DUX4-induced metabolic changes is lacking.

Here we pinpoint the kinetic involvement of altered mitochondrial ROS metabolism and impaired mitochondrial function in aetiology of oxidative stress in FSHD. Transcriptomic analysis in FSHD muscle biopsies reveals strong enrichment for pathways involved in mitochondrial complex I assembly, nitrogen metabolism, oxidative stress response and hypoxia signalling. We found elevated mitochondrial ROS (mitoROS) levels correlate with increases in steady-state mitochondrial membrane potential in FSHD myogenic cells. DUX4 triggers mitochondrial membrane polarisation prior to oxidative stress generation and apoptosis through mitoROS, and affects mitochondrial health through lipid peroxidation. We identify complex I as the primary target for DUX4-induced mitochondrial dysfunction, with strong correlation between complex I-linked respiration and cellular oxygenation/hypoxia signalling activity in environmental hypoxia. Thus, FSHD myogenesis is uniquely susceptible to hypoxia-induced oxidative stress as a consequence of metabolic mis-adaptation. Importantly, mitochondria-targeted antioxidants rescue FSHD pathology more effectively than conventional antioxidants, highlighting the central involvement of disturbed mitochondrial ROS metabolism. This work provides a pathomechanistic model by which DUX4-induced changes in oxidative metabolism impair muscle function in FSHD, amplified when metabolic adaptation to varying O_2 tension is required.

* Corresponding author.
** Corresponding author.
E-mail addresses: philipp.heher@kcl.ac.uk (P. Heher), peter.zammit@kcl.ac.uk (P.S. Zammit).

https://doi.org/10.1016/j.redox.2022.102251
Received 23 December 2021; Accepted 25 January 2022
Available online 29 January 2022

1. Introduction

Facioscapulohumeral muscular dystrophy (FSHD) is an incurable, hereditary disease primarily affecting skeletal muscle. FSHD is the third most common inherited muscular dystrophy, with an estimated prevalence of 4–12 in 100,000 [1,2]. FSHD presents as a descending, often left/right asymmetric, skeletal muscle weakness and atrophy, starting in facial muscles such as orbicularis oculi and orbicularis oris, and progressing to muscles of the shoulder girdle/proximal arm, before affecting specific lower limb muscles [3,4]. Fortunately, life-span is not attenuated, but FSHD severely affects quality of life, as approximately 30% of patients become wheelchair-bound while a further 10% require leg braces [3,5]. The FSHD clinical phenotype also extends to extra-muscular features including high-frequency hearing loss that is often sensorineural and may progress to deafness [6], and/or retinal telangiectasia (Coat's disease), a condition where abnormal vascular growth in the macula causes progressively compromised vision [7]. FSHD is a highly heterogeneous pathology, with presentations varying dramatically between first-degree relatives and even mono-zygotic twins [8,9]. Furthermore, males and females exhibit differential penetrance, with males usually presenting in the second decade of life while females are typically affected by the third [10].

The genetic cause underlying FSHD pathogenesis is epigenetic derepression of the subtelomeric *D4Z4* macrosatellite repeats on chromosome 4q35 [4,11]. Each *D4Z4* unit contains an open reading frame for the *Double Homeobox 4 (DUX4)* retrogene, encoding the homeobox transcription factor DUX4 (OMIM 606009) [12,13]. Approximately 95% of FSHD cases are classified as FSHD1 (OMIM 158900) and associated with contraction from the usual 11–100 repeats to <10 and epigenetic derepression of the *D4Z4* repeat region in the subtelomere of "permissive" chromosome 4qA allelic variants [14–16]. Along with reduced repressive histone modifications, CpG/DNA hypomethylation results in transcription of DUX4-full length from the otherwise somatically repressed distal-most *D4Z4* unit [17]. A polymorphism in FSHD-permissive 4qA haplotypes (4qA161 and rarer 4qA159 and 4qA168) provides a polyadenylation signal (PAS) for *DUX4* transcripts, allowing their stabilisation and translation [18]. Residual number of D4Z4 units inversely correlates with disease severity but at least one unit is needed for FSHD pathology [19]. FSHD2 (OMIM 158901) accounts for the remaining 5% of cases, which are mostly characterised by epigenetic derepression at *D4Z4* through mutations in *Structural maintenance of chromosomes flexible hinge domain containing 1 (SMCHD1)* [20], and much more rarely with mutations in *DNA methyltransferase 3B (DNMT3B)* [21] or the SMCHD1 protein interactor *ligand-dependent nuclear receptor-interacting factor 1 (LRIF1)* [22]. *SMCHD1* encodes a chromatin modifier that controls and maintains CpG methylation patterns for inheritable epigenetic silencing, for example during X-chromosome inactivation [23]. FSHD2 patients, however, also have *D4Z4* repeat numbers towards the shorter end of the normal range (<20 repeats) on permissive 4qA haplotypes, so that hypomethylation again permits *DUX4* expression from the distal-most *D4Z4* unit [20,21].

These two genetically distinct FSHD1 and FSHD2 subtypes are currently diagnosed by clinical and genetic means [24]. However, molecular analysis of the *D4Z4* locus in patient cohorts reveals that association between the number of D4Z4 repeats and clinical severity is not straightforward. Interestingly, an estimated 3% of the general population carrying *D4Z4* alleles in the FSHD size range (4–8 repeat units) does not suffer from the disease [25]. That individuals with 7–10 *D4Z4* repeats show low penetrance and present incomplete or atypical clinical phenotypes, including facial muscle sparing and/or normal motor function, adds complexity to establishing clinically and therapeutically relevant genotype-phenotype correlations [26,27].

While the genetics of FSHD have been studied in detail, much less is known about disease pathomechanisms. One of the most drastic consequences of aberrant *DUX4* expression is apoptosis, possibly through the p53-p21 axis [17,28,29] but molecular pathways are elusive. Further, DUX4 interferes with myogenic differentiation by inducing a more stem-cell-like transcriptional program [30], so likely impinging on both developmental and regenerative myogenesis. DUX4 leads to rapid downregulation of the transcription factors MyoD and Myf5, two key muscle regulatory factors (MRFs) [31,32]. *MyoD* is a Paired Box 7 (PAX7) target gene, and sequence similarity between the single PAX7 and two DUX4 homeodomains suggests that DUX4 interferes with the transcriptional circuitry controlled by PAX7 [32]. Indeed, a PAX7 target gene score is globally repressed in FSHD biopsies [33], with PAX7 target gene score repression a potent biomarker for FSHD [34].

Oxidative stress is a well-known pathomechanism of muscle diseases, with redox imbalances in several disorders such as Duchenne muscular dystrophy (DMD) [35,36], myotonic dystrophy type 1 (DM1) [37] and limb-girdle muscular dystrophy (LGMD) [38,39]. A pioneering study by Winokur et al. [40] revealed that FSHD myoblasts show a transcriptional dysregulation of the oxidative stress response, specifically with robust downregulation of antioxidant enzymes involved in the glutathione-based redox system. FSHD myoblasts have higher susceptibility to exogenously induced oxidative stress than controls, a susceptibility not seen in cellular models of other muscular dystrophies. Since this seminal observation of a unique oxidative stress-related pathomechanism in FSHD, oxidative stress/damage and mitochondrial dysfunction have been established as hallmarks of the disease. Several other *in vitro* studies have found perturbations of oxidative stress response and cellular bioenergetic pathways on the mRNA and protein level [41–46]. Although FSHD myoblasts are generally capable of repairing moderate oxidative damage, they fail to do so when oxidative stress becomes high and/or chronic [47]. It is, however, unclear whether reduced capacity of cellular antioxidant systems and/or chronically increased levels of reactive oxygen (RONS, or ROS) and nitrogen (RNS) species trigger oxidative damage in FSHD. FSHD myoblasts show elevated ROS levels and oxidative DNA damage, which can be reduced by antioxidant treatment [48]. Likewise, footprints of oxidative stress/damage have been identified in FSHD patients, both intramuscular (lipid peroxidation, lipofuscin accumulation, altered protein carbonylation) and systemic (reduced antioxidant levels in blood) [46]. DUX4 confers susceptibility to oxidative stress-induced cell death, and DUX4 increases ROS levels which are rescued by DUX4 knockdown or administration of antioxidants [32].

Skeletal muscle has high metabolic activity, so myofibres have to constantly adapt and respond to intrinsic and microenvironmental changes in their redox and bioenergetic regulatory pathways to meet energy demand. Since dynamic interplay between RONS, mitochondria and O_2/hypoxia signalling is core to muscle metabolic adaptation, chronic insult to the fine balance between pro- and antioxidant redox-mechanisms will lead to metabolic stress [49,50].

Mitochondrial dysfunction in FSHD pathogenesis is under studied. A respirometric study on patient muscle biopsies by Turki et al. [46] identified reduced cytochrome C oxidase (COX) activity and adenosine triphosphate (ATP) production in FSHD muscles, along with a decreased ratio between reduced and oxidized glutathione (GSH/GSSG). Both systemic oxidative stress and mitochondrial dysfunction correlated with muscle functional impairment, emphasising the central role of metabolic stress in FSHD. Further, different levels of proteins involved in mitochondrial oxidative metabolism have been found between healthy, DMD and FSHD muscle, most notably complex I subunits such as NADH dehydrogenase flavoprotein (NDUFV) and NADH-ubiquinone oxidoreductase (NDUFA), as well as the mitochondrial uncoupler adenine nucleotide translocator 1 (ANT1) [43]. Increased ANT1 correlates with enhanced ROS production and receptor of advanced glycation end products (RAGE) and nuclear factor kappa B (NF-κB) activity [44], suggesting mitochondrial involvement in pro-apoptotic signalling in FSHD muscle degeneration.

Both developmental and regenerative myogenesis are redox-sensitive and metabolic stress is a well-established negative regulator of myogenic differentiation [51]. *In vitro*, FSHD myotubes show

morphologic features of aberrant differentiation, evident as a disorganized or hypotrophic phenotype [52,53]. We have recently shown that differentiating FSHD myoblasts fail to fully activate a key mediator of mitochondrial biogenesis, the peroxisome proliferator-activated receptor gamma (PPARγ) coactivator 1α/estrogen-related receptor α (PGC1α/ERRα) axis, resulting in FSHD myotube hypotrophy [52]. PGC1α overexpression or treatment with ERRα agonists effectively rescues this FSHD hypotrophic phenotype, suggesting that mitochondrial (dys)function is central to impaired FSHD myogenesis. Since mitochondria are the main site of cellular O_2 consumption, hypoxia signalling and metabolic adaptation to varying O_2 availability might be directly affected by oxidative stress and dysfunctional FSHD mitochondria. We have previously also found perturbed hypoxia-inducible factor 1α (HIF1α) signalling in FSHD muscle biopsies [33,54], and a recent study identifies HIF1α signalling as the main driver of DUX4-induced muscle cell death [55].

Although unclear how altered muscle cell metabolism, oxidative stress and hypoxia signalling are involved in FSHD pathogenesis at the molecular level, antioxidant treatment has been proposed as a potential therapy for FSHD [56]. Antioxidants rescue aspects of DUX4 toxicity, such as oxidative DNA damage [48] and apoptosis [57], possibly by suppressing *DUX4* transcription itself, which increases under oxidative stress through a DNA damage response-dependent mechanism [58]. A clinical trial evaluating dietary antioxidant supplementation (vitamin C, vitamin E, zinc gluconate and selenomethionine) in FSHD patients demonstrated moderate muscle functional improvement with a concomitant alleviation of oxidative stress and damage [59,60].

To date, only conventional, non-targeted antioxidants that mainly accumulate in the cytoplasm have been investigated. Since the respiratory chain can be a significant driver of ROS formation, especially in dysfunctional mitochondria, more targeted antioxidant-based therapeutic approaches might improve the so far rather moderate clinical outcomes. Indeed, a recent study [61] has shown that mitochondria-targeted antioxidant treatment in muscle cells with a low level of DUX4-induction can partially rescue aspects of DUX4-induced redox and differentiation defects, suggesting a role of mitochondrial ROS (mitoROS) in DUX4 toxicity.

Our aim is to understand how disturbed redox signalling and muscle metabolism integrate into current pathophysiologic paradigms to identify how mitochondria contribute to metabolic stress in FSHD. Our differential gene expression analysis of published RNA sequencing (RNAseq) data of FSHD muscle biopsies [62] reveals strong enrichment of genes involved in processes related to mitochondria, with mitochondrial complex I (NADH dehydrogenase) assembly being the top differentially expressed gene ontology (GO) term. We identify that elevated mitochondrial membrane potential (ΔΨm) correlates with increased ROS levels in a panel of FSHD patient-derived muscle lines, which produce hypotrophic FSHD myotubes. DUX4 increases ΔΨm and ROS in a dose-dependent manner. Importantly, DUX4-induced changes in mitochondrial function and metabolic activity precede oxidative stress through mitoROS formation, identifying mitochondria as the source of excess ROS. Respirometric analysis of DUX4-overexpressing muscle cells reveals that, in accordance with the transcriptomics data, complex I is the main target conferring mitochondrial dysfunction, while complex II-linked respiration is largely unaffected. DUX4 also differentially affects HIF1α stabilisation under environmental hypoxia in myoblasts versus myotubes, emphasising the relation between mitochondrial respiration and hypoxia signalling. HIF1α stabilisation correlates with complex I-linked respiration, in a manner involving both cellular redistribution of O_2 and mitoROS. DUX4-induced perturbation of cellular respiration and hypoxia signalling sensitizes FSHD myogenesis to hypoxia through increased oxidative stress, evident by hypoxia-induced increases in ΔΨm and ROS levels that aggravate the hypotrophic myotube phenotype compared to normoxia. Finally, we show that antioxidant treatment of differentiating FSHD muscle cells rescues FSHD myogenesis in hypoxia through alleviation of oxidative stress. Intriguingly, although all tested antioxidants rescue FSHD myotube hypotrophy, the mitochondria-targeted superoxide ($O_2^{\bullet-}$) dismutase (SOD) mimetic mitoTEMPO is most efficient, not only reducing ROS levels but also ΔΨm and cellular hypoxia while increasing metabolic activity. This work suggests that oxidative stress and hypoxia signalling perturbation in FSHD are caused by mitochondrial dysfunction, and that mitochondria-targeted antioxidants may offer a novel therapeutic entry point to complement the current, more experimental therapies directed at reducing DUX4 levels.

2. Results

2.1. Transcriptional deregulation of pathways involved in the mitochondrial respiratory chain in FSHD muscle biopsies and patient-derived FSHD muscle cells

We have previously shown that genes involved in oxidative phosphorylation (OXPHOS), mitochondrial aerobic metabolism and mitochondrial biogenesis are dynamically repressed in FSHD myogenesis [52]. Here, to examine interplay between mitochondria, ROS metabolism and hypoxia signalling, we re-analysed previously published RNAseq data (GSE115650) from magnetic resonance imaging (MRI)--guided FSHD muscle biopsies recently published by Wang et al. [62] (patient demographics, genetics, pathology and MRI-features are detailed in Ref. [62]). Wang et al. stratified their FSHD patients on the basis of increasing relative expression of four DUX4 target genes (*LEUTX, KHDC1L, TRIM43* and *PRAMEF2*) into Groups 1 to 4 [62]. Group 4 showed active pathology in the form of muscle fibre necrosis/regeneration or inflammation [62].

We identified 7035 differentially expressed genes (DEG), with 3147 down-regulated and 3888 up-regulated in muscle biopsies from the 6 FSHD patients with the highest relative expression of the four DUX4 target genes (Group 4 [62]), compared to the 9 control individuals (Fig. 1A). GO analysis identified significantly enriched biological processes related to mitochondria, response to oxidative stress and O_2 levels, and metabolism of nitrogen compounds (Fig. 1B and C), regulated through differential expression of 887 genes in FSHD (Fig. 1D). Notably, among the 30 top significant GO terms: biological processes (GOBPs), genes involved in mitochondrial complex I assembly and mitochondrial gene expression were specifically enriched. In addition, genes involved in development of functional muscle, blood vessels and immune response were found enriched in FSHD (Fig. 1B and C), identifying extra-muscular pathological features.

Since the mitochondrial genome encodes important protein subunits involved in the respiratory chain [six complex I subunits (MT-ND1-6), one complex III subunit (MT-CYB), three complex IV subunits (MT-CO1-3) and two complex V subunits (MT-ATP6, 8) [63]], we also analysed expression of the 13 protein-coding mitochondrial genes based on DESeq2 normalized counts from this same published FSHD patient and unaffected individual cohort. In accordance with the GOBP analysis (Fig. 1B and C), most of the 13 mitochondrial protein-coding genes were downregulated in FSHD patient muscle from Groups 1–3, and all were significantly downregulated in Group 4 (Fig. 1E and Fig. S1). The relative expression of the DUX4 target genes *ZSCAN4*, *TRIM43*, *PRAMEF1* and *MBD3L2* were also highest in Group 4 (Fig. 1E). There was a significant inverse correlation between DUX4 target gene expression (*ZSCAN4*, *TRIM43*, *PRAMEF1* and *MBD3L2*) and that of the mitochondrially encoded protein-coding genes in patient biopsies with increasing pathological severity (Group 1–4) (Fig. 1F).

Downregulation of the 13 protein-coding mitochondrial genes was also significant in FSHD patient-derived myoblasts (16A) versus sibling-matched controls (16U) *in vitro*, and also able to distinguish the FSHD from the control line (Fig. 1G). Since complex I subunits encoded by both the mitochondrial and nuclear genome are affected, we hypothesised that mitochondrial dysfunction might predominantly stem from alterations in complex I-linked respiration (Fig. 1B).

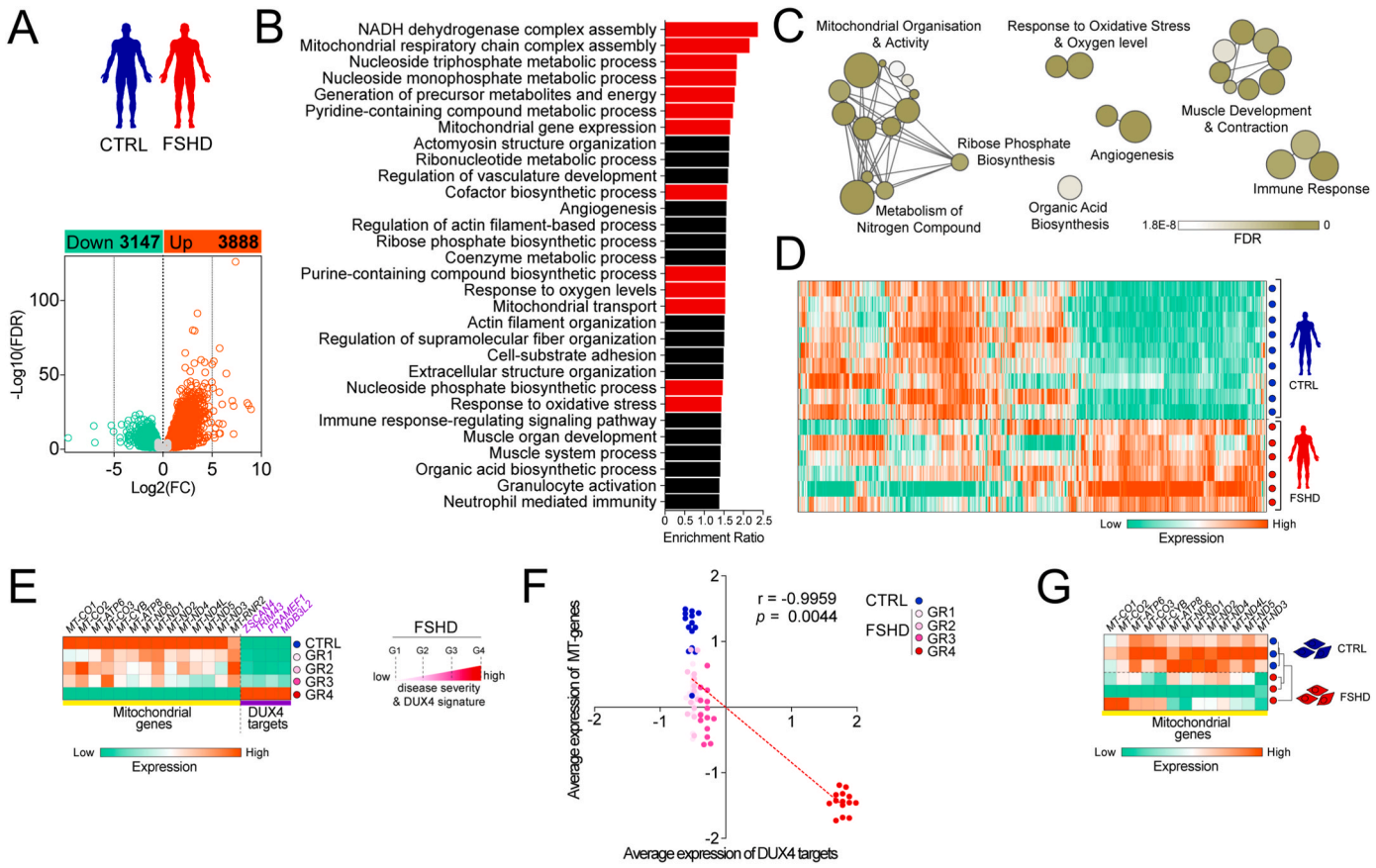

Fig. 1. ***Transcriptional deregulation of pathways involved in mitochondrial oxidative metabolism, oxidative stress and hypoxia signalling in FSHD muscle biopsies and myoblasts.*** **(A)** 7035 genes were differentially expressed, with 3147 down-regulated and 3888 up-regulated in RNASeq data (GSE115650 [62]) from muscle biopsies from 6 FSHD patients with severe pathology (Group 4), compared to 9 control individuals. **(B, C)** Gene ontology analysis reveals significantly enriched biological processes related to mitochondria, response to oxidative stress and O_2 levels and metabolism of nitrogen compounds (highlighted in red), **(D)** regulated through differential expression of 887 genes in FSHD. **(E)** Transcriptional downregulation of all protein coding genes encoded by the mitochondrial genome with increasing disease severity (as stratified by relative DUX4 target gene expression of *LEUTX, KHDC1L, TRIM43* and *PRAMEF2* [62]). **(F)** Robust correlation of DUX4 target gene expression with decrease in mitochondrial gene expression from low to high disease severity. **(G)** Transcriptional downregulation of all mitochondrial protein coding genes distinguishes myoblasts derived from an FSHD1 patient (16A) from an unaffected sibling-matched control (16U). (For interpretation of the references to colour in this figure legend, the reader is referred to the Web version of this article.)

2.2. FSHD myogenic cells are characterised by elevated steady-state ΔΨm and increased mitoROS levels

Since transcriptomic analysis showed widespread alterations in mitochondrial genes, we analysed the relationship between mitochondrial function characterised by ΔΨm and intracellular ROS metabolism in FSHD. ΔΨm is an important parameter of mitochondrial function, as is part of the proton motive force (pmf) maintained across the mitochondrial membrane to drive ATP synthesis through OXPHOS [64]. We examined ΔΨm in a panel of patient-derived FSHD myoblast cell lines and matched controls: the 54 and K series derived from two mosaic FSHD1 patients, and so isogenic bar the FSHD contraction, and 16s from an FSHD patient and their unaffected sibling. ΔΨm was significantly increased in FSHD muscle cells (54-12, K8 and 16A) compared to controls (54-6, K4, 16U), irrespective of stage of differentiation (myoblasts versus differentiated myotubes), as assayed with tetramethylrhodamine methyl ester (TMRM) fluorescence measurements (Fig. 2A).

Since the respiratory chain can produce large amounts of ROS at persistently high ΔΨm [65], we next assessed cytoplasmic ROS levels using the general ROS indicator CM-H_2DCFDA. We found consistently elevated ROS levels in FSHD myogenic cells, as assessed by CM-H_2DCFDA fluorescence measurements (Fig. 2B), correlating with increased ΔΨm. Intriguingly, probing for mitoROS levels with MitoTracker® Red CM-H_2XROS revealed that FSHD mitochondria are characterised by significantly higher ROS levels (Fig. 2C). This suggests that mitochondrial $O_2^{\bullet-}$ leaking from the electron transport chain (ETC) into the mitochondrial matrix and cytoplasm could be a major source contributing to oxidative stress generation in FSHD. This positive correlation between elevated ΔΨm and (mito)ROS levels was consistent between different patient-derived cellular models. Further, impaired mitochondrial ROS metabolism in FSHD myogenic cells correlates with formation of hypotrophic FSHD myotubes upon differentiation, as shown by immunolabelling for the sarcomeric protein myosin heavy chain (MyHC) (Fig. 2D; quantification of MyHC-containing area in Figs. 8E and S5). This supports our theory that redox imbalances in FSHD cells towards a gradually more oxidative cellular environment impair FSHD myogenesis.

2.3. DUX4-induced changes in mitochondrial function and metabolic activity precede oxidative stress through increased mitoROS formation

To investigate impact of DUX4 on modulation of mitochondrial activity and ROS metabolism, we used the DUX4-inducible LHCN-M2-iDUX (iDUX4) human myoblast line [66] to examine kinetics of redox changes in response to varying levels of DUX4. We titrated the doxycycline (DOX) inducer to elicit low (12.5 ng/mL DOX), medium (62.5 ng/mL DOX) and strong (125 ng/mL DOX) DUX4 induction. Similar to our observations in FSHD myoblasts, DUX4 induced an increase in ΔΨm

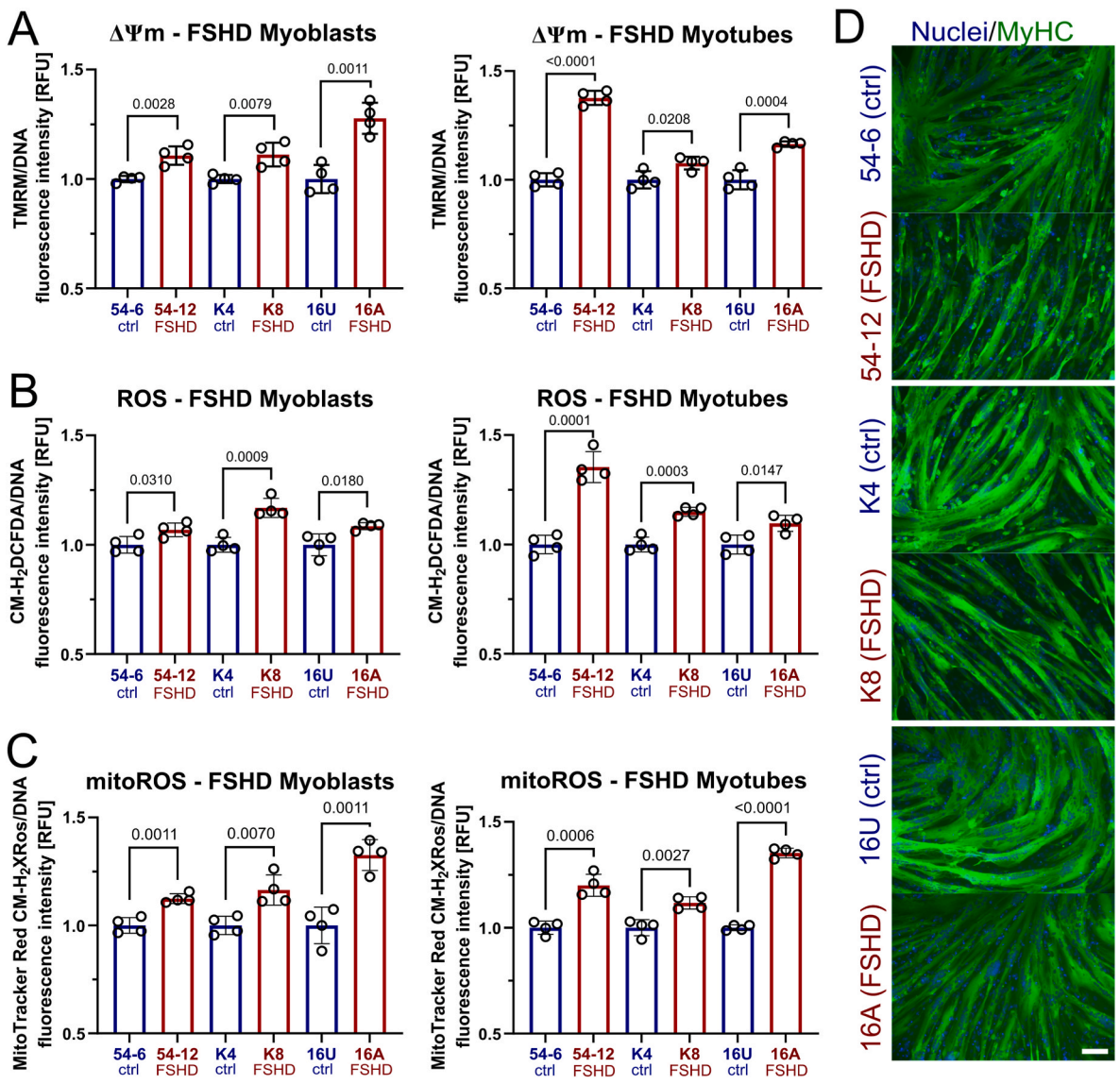

Fig. 2. ***Altered mitochondrial ROS metabolism in FSHD muscle cells correlates with increased ΔΨm and hypotrophic myotubes.*** **(A)** Consistently increased steady-state ΔΨm in mitochondria in 3 independent FSHD myoblast and myotube lines (54-6 ctrl/54-12 FSHD; K4 ctrl/K8 FSHD; 16U ctrl/16A FSHD), as assessed by measuring tetramethylrhodamine methyl ester (TMRM) fluorescence. **(B)** Increased general (cytoplasmic) ROS (assessed by CM-H_2DCFDA fluorescence) and **(C)** mitoROS levels (assessed by MitoTracker® Red CM-H_2XROS fluorescence) were found in the same human cell line pairs. **(D)** Upon myogenic differentiation, FSHD myotubes exhibit a hypotrophic phenotype compared to their isogenic/sibling control, as shown by immunolabelling for MyHC (green), with a nuclear HOECHST33342 (blue) counterstain (scale bar represents 100 μm). Data is mean ± s.d. from 3 independent cells pairs with 4 wells each from a representative experiment with *p* values as indicated. (For interpretation of the references to colour in this figure legend, the reader is referred to the Web version of this article.)

in a dose-dependent manner (Fig. 3A), with significant changes in ΔΨm detectable after 8 h with the highest DOX concentration (125 ng/mL) in iDUX4 myoblasts. After 12 h, all DUX4 induction treatments showed significant elevation of ΔΨm. Likewise, metabolic activity at the 12 h timepoint was significantly reduced at all DUX4 levels (Fig. S2A). Tracking ΔΨm and both general and mitoROS levels over the 16 h experimental period revealed interesting kinetics regarding DUX4-induced changes in mitoROS metabolism (Fig. 3A and B). DUX4 interferes with mitochondrial metabolic activity, highlighted by an initial decrease in general and mitoROS levels (8 h timepoint) and concomitant gradual polarisation of the mitochondrial membrane, likely through DUX4 adversely affecting OXPHOS. As the increase in ΔΨm becomes chronic and more pronounced (T12-16 h), a significant increase in mitoROS levels follows, detectable after 16 h with medium and strong DUX4 induction (Fig. 3B). Again, the concept that cytoplasmic and mitoROS levels showed similar kinetics in response to DUX4 expression highlights the central involvement of the respiratory chain in ROS production, which are eventually released from the mitochondrial matrix into the cytoplasm. Possibly, DUX4 affects both processes, the rate of mitoROS generation and their release into the cytoplasm via formation of mitochondrial permeability transition pores.

Given the known relationship between ΔΨm and mitoROS generation [64], even moderate increases in ΔΨm can drastically increase ROS levels, especially when these changes in ΔΨm become chronic and the oxidative stress response is gradually overwhelmed by excess mitoROS. Changes in ΔΨm preceded by at least 4 h increases in general (cytoplasmic) ROS (Fig. 3A) and mitoROS (Fig. 3B) in iDUX4 myoblasts at medium (62.5 ng/mL DOX) or strong (125 ng/mL DOX) DUX4 stimulation. Interestingly, low (12.5 ng/mL DOX) DUX4 induction did not trigger measurable increases in mitoROS levels over 16 h, albeit increasing ΔΨm significantly. Since the methodology used in this study measures ROS levels, not production, we therefore also assayed

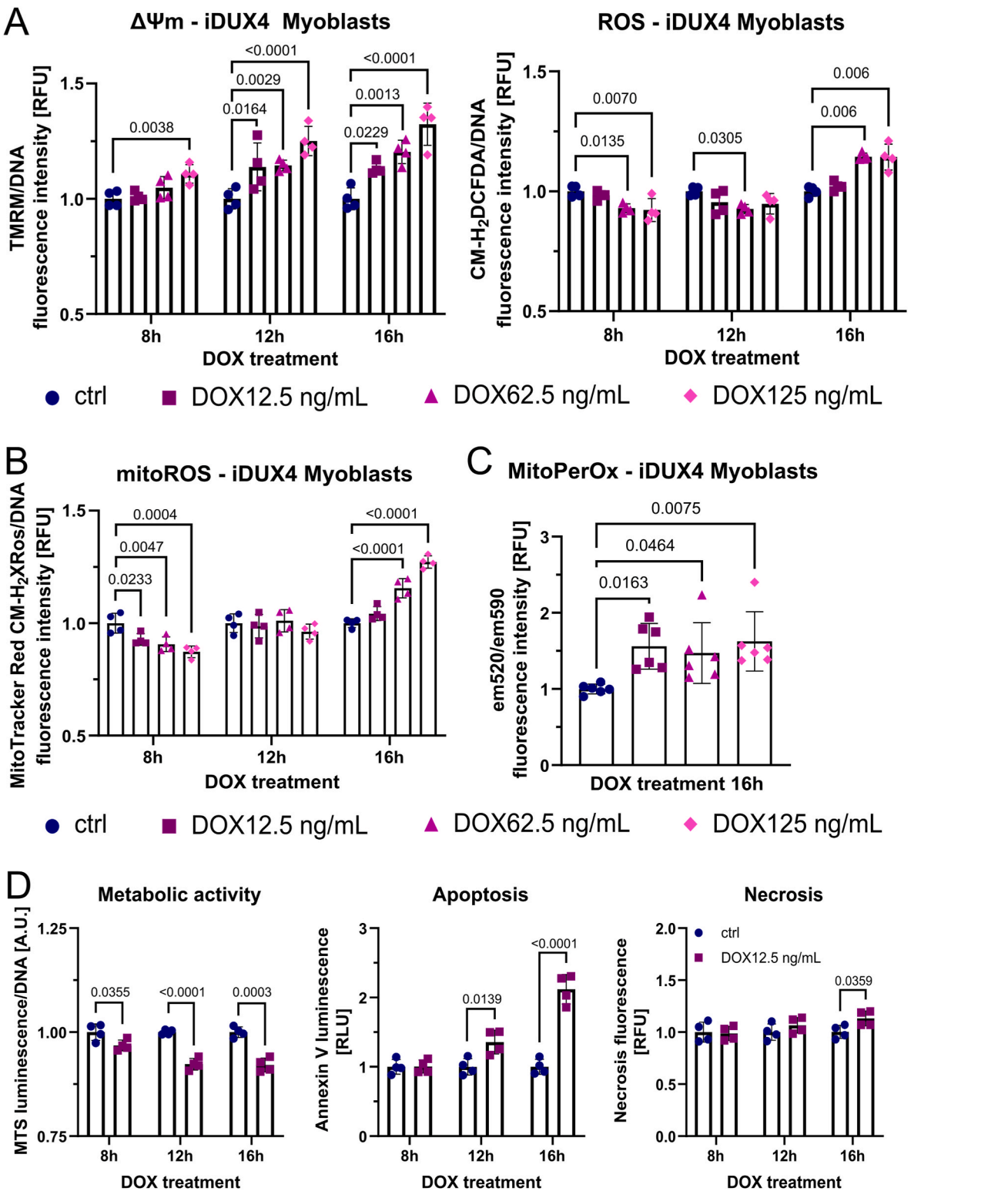

Fig. 3. ***DUX4-induced mitochondrial dysfunction is an early event in oxidative stress generation through mitochondrial ROS.*** **(A)** DUX4 increases ΔΨm in DUX4-inducible LHCN-M2-iDUX (iDUX4) human myoblasts in a dose dependent manner (assessed by TMRM fluorescence), preceding detection of elevated ROS levels (assessed by CM-H_2DCFDA fluorescence) by at least 4 h, and **(B)** subsequently triggers oxidative stress through mitochondrial ROS (assessed by MitoTracker® Red CM-H_2XROS fluorescence). **(C)** The gradual increase in mitoROS subsequently causes mitochondrial oxidative damage through lipid peroxidation after 16 h of DUX4 expression, quantified by calculating the ratio between MitoPerOx fluorescence intensity at em520/em590 after excitation at 488 nm. **(D)** Changes in metabolic activity (measured using the luminescence RealTime-Glo™ MT Cell Viability assay with normalisation to DNA content) precede apoptosis (measured using RealTime-Glo™ Annexin V Apoptosis and Necrosis assay), the main trigger of DUX4-induced muscle cell death, which commences after 12 h of low DUX4 expression. Data is mean ± s.d. from at least 4 wells each from a representative experiment with *p* values as indicated.

mitochondrial lipid peroxidation (calculated by the ratio between MitoPerOx fluorescence intensity at em520/em590 after excitation at 488 nm) to investigate whether even low induction of DUX4 is capable of contributing to mitochondrial oxidative damage through mitoROS (Fig. 3C). As hypothesised, after 16 h of DUX4 induction at variable intensity, all DUX4 levels led to significantly increased mitochondrial lipid peroxidation at comparable levels, compared to non-induced controls, suggesting that low induction of DUX4 does increase mitoROS generation from the respiratory chain.

To investigate the temporal relationship between metabolic stress and cell death in more detail, we used low DUX4 induction (12.5 ng/mL DOX) to track changes in metabolic activity and apoptosis/necrosis. DUX4 led to an immediate decrease in metabolic activity, measured using the luminescence RealTime-Glo™ MT Cell Viability assay with normalisation to DNA content, already evident at the earliest 8 h timepoint of DOX stimulation, so before significant increases in ΔΨm could be detected. Using the combined luminescence/fluorescence RealTime-Glo™ Annexin V Apoptosis and Necrosis assay to detect early apoptosis revealed that the first signs of apoptosis were evident around 12 h, and more pronounced at 16 h (Fig. 3D). However, morphologically, DUX4 induction with 12.5 ng/mL DOX did not show an overt apoptotic phenotype over 16 h (Fig, S2C), suggesting that the majority of cells were in the early stages of apoptosis. Apoptosis seems to be the driving force of DUX4 toxicity, although a moderate increase in necrosis could also be detected. As expected, apoptosis and necrosis correlated with the degree of DUX4 induction (Figs. S2B and C), as did (mito)ROS levels and ΔΨm (Fig. 3A and B) in iDUX4 myoblasts. After 16 h, Annexin V signal was significantly increased at all DUX4 levels, but correlating morphological changes only occurred at medium (62.5 ng/mL DOX) or strong (125 ng/mL DOX) DUX4 stimulation, which further correlated with a concomitant significant increase in necrosis and decrease in DNA content (Figs. S2B and C). Since these two treatment groups were also marked by elevated (mito)ROS levels, DUX-induced apoptosis likely involves mitochondrial pro-apoptotic signalling in response to persistent mitochondrial oxidative damage. This is further substantiated by the observation that, after the onset of apoptosis (24 h), all DUX4 stimulation regimes triggered a gradual collapse of ΔΨm with a concomitant decrease in ROS levels, likely due to cell death in response to mitochondrial dysfunction (Fig. S2D).

To examine whether effects of DUX4 on ΔΨm and mitoROS metabolism are consistent between iDUX4 myoblasts and myotubes, we induced DUX4 expression at variable levels in iDUX4 myotubes. We obtained similar results compared to myoblasts, but overall higher DUX4 levels were needed, as myotubes mainly rely on OXPHOS [67] and are thus generally better equipped to cope with resulting oxidative stress [68,69]. Increase in ΔΨm in response to variable DUX4 levels was dose-dependent, with strong induction (125 ng/mL DOX) leading to a significant increase after 12 h, with elevated ROS levels evident after 24 h of DOX treatment in iDUX4 myotubes (Fig. 4A). Likewise, the 24 h timepoint coincided with an increase in mitoROS levels at 125 ng/mL DOX (Fig. 4B). mitoROS levels in iDUX4 myotubes were unchanged 12 h after DUX4 induction, followed by increased levels as mitochondrial membrane polarisation progresses (Fig. 4B).

Again, mitochondrial oxidative damage, as assessed via mitochondrial lipid peroxidation (Fig. 4C), and concomitantly reduced metabolic activity (Fig. 4D) was triggered at all DUX4 levels in iDUX4 myotubes after 24 h, pointing to similar mechanisms of DUX4-induced redox disturbances to those operating in iDUX4 myoblasts.

These data suggest the impairment of mitochondrial OXPHOS as an early event in DUX4-induced toxicity, leading to a gradual increase in ΔΨm, which in turn manifests in mitochondrial oxidative damage caused by an excess of mitoROS. Once the (mitochondrial) oxidative stress response is overwhelmed in response to these chronic redox changes, mitochondrial dysfunction (collapse of ΔΨm and decrease of ROS in response to reduced OXPHOS), at least in part, triggers apoptosis.

2.4. DUX4-induced mitochondrial dysfunction is conferred through mitochondrial complex I

Having identified DUX4 as a major trigger of changes in ΔΨm and mitochondrial ROS metabolism, and the similarity of these changes between FSHD patient-derived, and iDUX4 disease, models, we next investigated effects of DUX4 on mitochondrial oxygen consumption through high-resolution respirometry. Normally, complex I contributes to generation of ΔΨm, so increased ΔΨm in FSHD might be attributable to altered complex I activity, as suggested by our transcriptomic analysis (Fig. 1). Thus, we next focussed on how DUX4 affects mitochondrial respiration if electrons to the ETC are provided via either complex I or II.

We induced DUX4 in iDUX4 myoblasts with 62.5 ng/mL DOX for 16 h, a concentration that robustly increases ΔΨm and (mito)ROS levels (Fig. 3A and B). DUX4 significantly reduced complex I-linked OXPHOS (state 3) and maximum electron transfer system (ETS) capacity in iDUX4 myoblasts, while complex II-linked respiration was unaffected (Fig. 5A–C). LEAK respiration (state 4) via complex I was also reduced (Fig. 5D), possibly contributing to mitoROS generation through mitochondrial membrane hyperpolarisation. LEAK respiration via complex II was unchanged (Fig. S3A), as were the respiratory control ratio (RCR) of both complex I and II (Fig. S3B). Representative oxygraphs are shown in Fig. S3C.

Complex I-linked respiration was also primarily affected by DUX4 expression in iDUX4 myotubes with 62.5 ng/mL DOX for 24 h. However, DUX4 expression caused an increase in both complex I-linked OXPHOS (state 3) and maximum ETS capacity in iDUX4 myotubes, while these parameters where largely unchanged via complex II (Fig. 5E–G). In contrast to iDUX4 myoblasts, LEAK respiration via complex I (state 4) was unaffected (Fig. 5H), as was LEAK respiration through complex II (Fig. S3D). RCR of both complex I and II was moderately increased (Fig. S3E). Representative oxygraphs are shown in Fig. S3F. Myoblast viability or DNA content of sister myotube cultures were used for normalisation (Fig. S3G).

2.5. DUX4-induced mitochondrial dysfunction conferred through mitochondrial complex I interferes with hypoxia signalling

We next focused on the link between mitochondrial dysfunction and deregulated hypoxia signalling [54,55]. Dysfunctional mitochondria with altered oxygen consumption rates can directly affect HIF1α nuclear stabilisation through mechanisms including redistribution of cellular O_2 and ROS signalling [70–72]. We cultured iDUX4 myoblasts and myotubes in environmental hypoxia (1% O_2) and induced DUX4 as per the respirometry experiments. Altered mitochondrial function correlated with cellular oxygenation, as assessed by the fluorescent O_2-sensitive hypoxia indicator Image-IT™ Green Hypoxia Reagent: DUX4 expressing myoblasts (with reduced complex I-linked respiration) were marked by higher intracellular O_2 levels (and were thus less hypoxic), whereas myotubes (with increased complex I-linked respiration) displayed lower intracellular O_2 levels (and were thus more hypoxic), as assessed with fluorescence intensity measurements using a hypoxia sensitive fluorescent dye (Fig. 5I).

Differential regulation of the molecular response to hypoxia in 1% O_2 was further supported by the finding that DUX4 and nuclear-located HIF1α protein inversely correlate in myoblasts. Increasing DOX

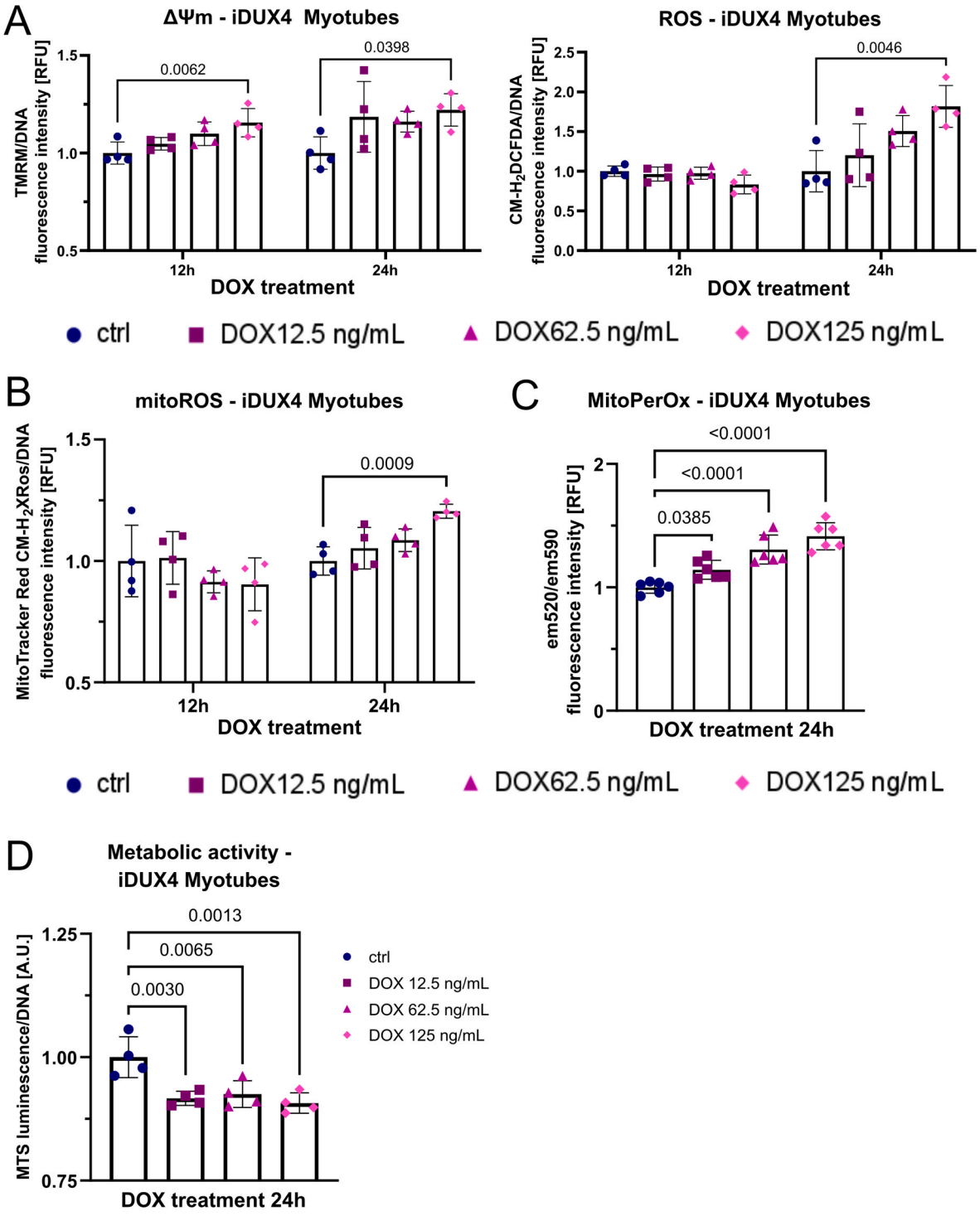

Fig. 4. ***DUX4 expression in myotubes impacts mitochondrial function and subsequently perturbs ROS metabolism.*** **(A)** High DUX4 expression increases ΔΨm in iDUX4 myotubes (assessed by measuring TMRM fluorescence), preceding detection of elevated ROS levels (assessed by CM-H_2DCFDA fluorescence) by 12 h, and subsequently triggers **(B)** oxidative stress through mitochondrial ROS (assessed by MitoTracker® Red CM-H_2XROS fluorescence). **(C)** The gradual increase in mitoROS causes mitochondrial oxidative damage after 24 h of DUX4 expression, with mitochondrial lipid peroxidation quantified by calculating the ratio between MitoPerOx fluorescence intensity at em520/em590 after excitation at 488 nm. **(D)** Similar to changes in myoblasts, DUX4 expression for 24 h in myotubes causes reduction of metabolic activity (measured using the luminescence RealTime-Glo™ MT Cell Viability assay with normalisation to DNA content) as oxidative stress through elevated ROS becomes evident. Data is mean ± s.d. from 4 wells each from a representative experiment with *p* values as indicated.

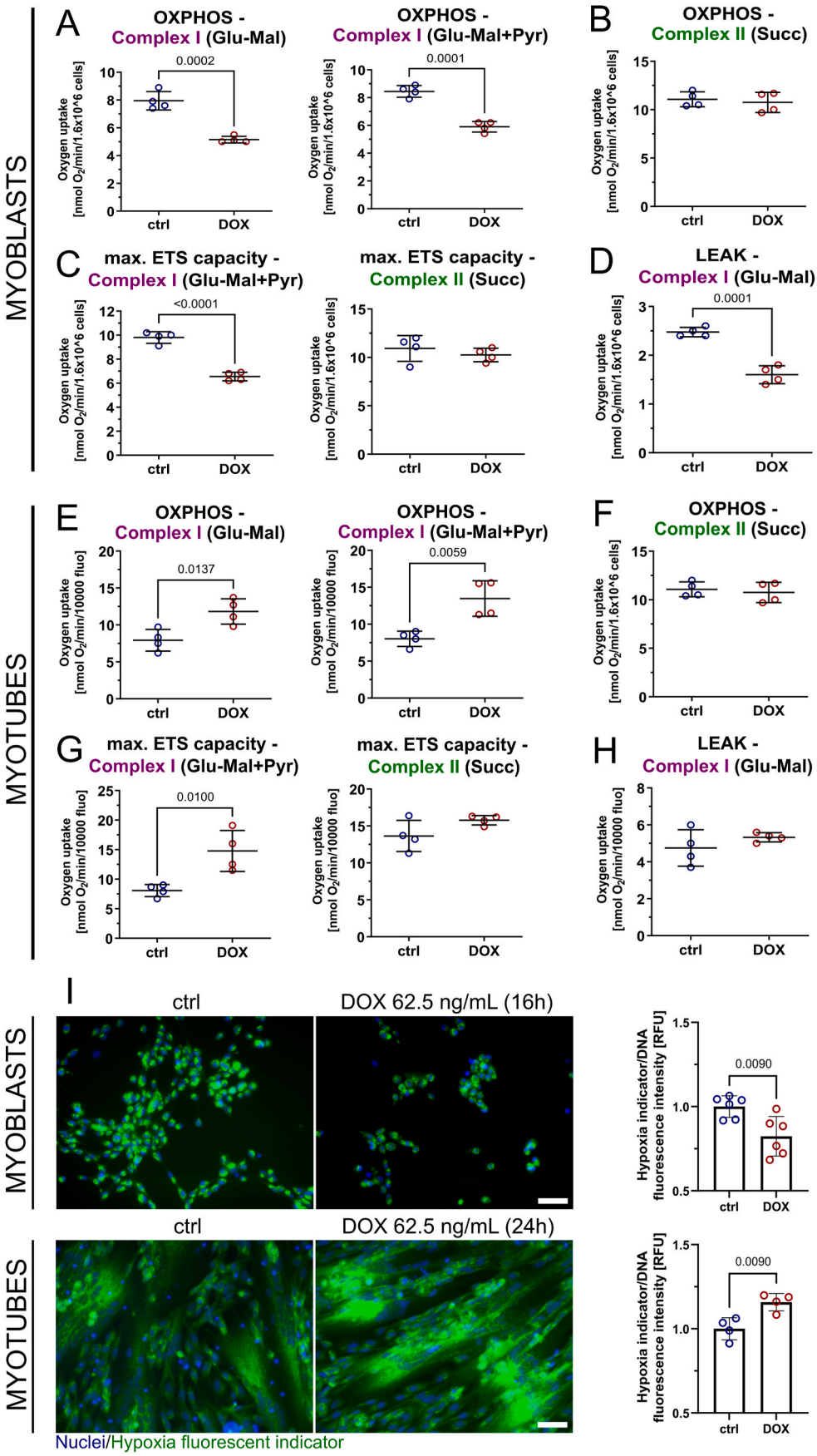

Fig. 5. ***DUX4 affects mitochondrial respiration specifically at complex I and impairs cellular oxygenation through cellular redistribution of O_2.*** **(A–D)** High-resolution respirometry in DUX4 expressing iDUX4 myoblasts (DOX 62.5 ng/mL for 16 h) identifies reduced OXPHOS, maximum electron transfer system (ETS) capacity and LEAK (uncoupled) respiration through complex I, but not complex II. **(E–G)** Complex I-linked OXPHOS and maximum ETS capacity is increased in DUX4 expressing myotubes (DOX 62.5 ng/mL for 24 h), while complex II is again unaffected. **(H)** In contrast to myoblasts, DUX4 does not change complex I LEAK respiration in iDUX4 myotubes. Glu: 5 mM glutamate, Mal: 5 mM malate, Pyr: 10 mM pyruvate, Succ: 10 mM succinate/1.4 μM rotenone. **(I)** Hypoxia indicator fluorescence microscopy using the fluorescent O_2-sensitive hypoxia indicator Image-IT™ Green Hypoxia Reagent of DUX4 expressing iDUX4 myoblasts (top panel) and myotubes (bottom panel) grown in hypoxia (1% O_2) reveals correlation between complex I-linked respiration and cellular hypoxia, as quantified by indicator dye fluorescence intensity on a plate reader in a separate experiment (representative micrographs are shown, scale bar represents 50 μm). Data is mean ± s.d. from 4 to 6 wells each from a representative experiment (except for respirometry, where 4 independent experiments were performed) with p values as indicated. (For interpretation of the references to colour in this figure legend, the reader is referred to the Web version of this article.)

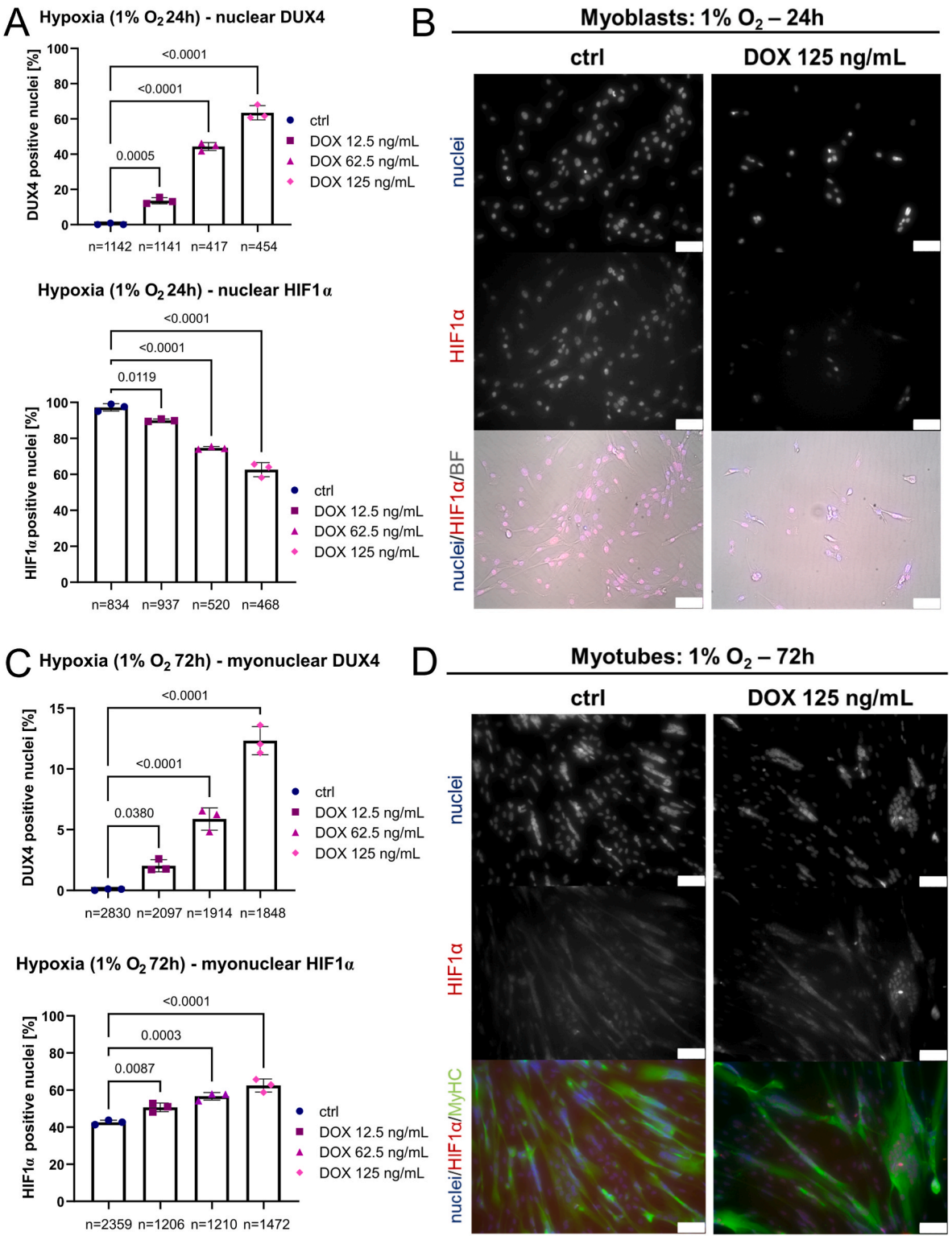

Fig. 6. ***DUX4 interferes with HIF1α signalling activity in environmental hypoxia.*** **(A)** Percentage of DUX4-positive and HIF1α-positive nuclei in hypoxic iDUX4 myoblasts under 1% O_2 induced to express DUX4 for 24 h at variable levels correlate inversely, with reduced nuclear HIF1α correlating with reduced complex I-linked OXPHOS (see Fig. 5A–D). **(B)** Representative immunofluorescence microscopy image of iDUX4 myoblasts after DUX4 expression (DOX 125 ng/mL for 24 h) in hypoxia immunolabelled for HIF1α, with a nuclear HOECHST33342 counterstain, alongside non-induced controls (BF: brightfield, scale bar represents 75 μm). **(C)** Percentage of DUX4-positive myonuclei in hypoxic myotubes under 1% O_2 induced to express DUX4 for 24 h at variable amounts correlates with HIF1α nuclear localisation and with increased complex I-linked OXPHOS (see Fig. 5E–G). **(D)** Representative immunofluorescence microscopy image of iDUX4 myotubes after DUX4 expression (DOX 125 ng/mL for 24 h) in hypoxia (differentiation for 72 h under 1% O_2) co-immunolabelled for HIF1α and MyHC, with a nuclear HOECHST33342 counterstain, alongside non-induced controls (scale bar represents 75 μm). Data is mean ± s.d. of number of nuclei/myonuclei stated, from 3 wells from a representative experiment with *p* values as indicated. (For interpretation of the references to colour in this figure legend, the reader is referred to the Web version of this article.)

concentrations (12.5 vs 62.5 vs 125 ng/mL DOX for 24 h) reduced HIF1α-positive nuclei from ~100% in uninduced hypoxic iDUX4 myoblasts to ~60% at the highest DUX4 levels, as assessed by immunofluorescence (Fig. 6A and B). Conversely, DUX4 induction for 24 h in hypoxic iDUX4 myotubes under 1% O_2 increased the percentage of HIF1α-positive myonuclei from about 40% in uninduced controls to 60% at the highest DOX levels (Fig. 6C and D). Low to medium DUX4 induction in iDUX4 myotubes also led to significant changes in nuclear HIF1α in a dose-dependent manner, suggesting that DUX4 acts on HIF1α signalling activity in a mechanism involving mitochondria.

2.6. DUX4 aggravates hypoxia-induced oxidative stress and sensitizes FSHD myogenesis to hypoxia

Having shown that DUX4 alters mitochondrial function and interferes with HIF1α activation, we next investigated the effects of DUX4 on ΔΨm and ROS levels in hypoxia. Myogenic differentiation is characterised by a gradual switch from predominantly glycolytic metabolism in myoblasts to OXPHOS in myotubes as the major energy source, and perturbation of metabolic pathways required for oxidative metabolism impacts myogenic differentiation [73,74]. Skeletal muscles are subject to regular physiological variations in local O_2 availability, and hypoxia signalling is central to metabolic adaptation. Thus DUX4-induced redox and metabolic changes will interfere with this normal adaptation to hypoxia, a condition that naturally elicits some degree of oxidative stress [75].

We analysed ΔΨm and ROS levels in iDUX4 myoblasts and myotubes cultured in ambient ("normoxia", 21% O_2) versus hypoxic (1% O_2) conditions. Hypoxia increased both ΔΨm and ROS levels in non-induced iDUX4 myoblasts and ROS levels in non-induced iDUX4 myotubes. DUX4 increased ΔΨm and ROS levels in normoxia, and they were further enhanced at 1% O_2 in both iDUX4 myoblasts and myotubes treated with 125 ng/mL DOX (Fig. 7A and B). Consequently, myogenic differentiation was affected at lower levels of DUX4 induction in hypoxia compared to normoxia. Non-induced control iDUX4 myoblasts differentiated into myotubes with similar efficiency at 21% versus 1%, so regardless of O_2 availability. However, myogenesis was impaired at lower DOX concentrations (so lower DUX4 levels) in hypoxia (62.5 ng/mL DOX) compared to normoxia (125 ng/mL DOX), as assessed by quantification of MyHC-containing area (Fig. 7C and D). While high DUX4 induction with 125 ng/mL DOX elicited myotube hypotrophy both under normoxic and hypoxic conditions after 24 h, medium induction (62.5 ng/mL DOX) only produced this phenotype in hypoxia (Fig. 7D). Morphologically, this phenotype was accompanied by iDUX4 myotube fragmentation and increased presence of hypotrophic myotubes with myonuclei strongly positive for HIF1α (Fig. S4). Morphological myotube hypotrophy/fragmentation correlated with increased mitoROS levels, which were only evident at DOX concentrations that produced a hypotrophic phenotype (Fig. 7E).

We next assessed effects of hypoxia (1% O_2) on the three independent patient-derived FSHD/control paired myoblast lines. FSHD myotubes maintained higher ΔΨm and ROS levels in hypoxia (Fig. 8A and B), with more pronounced differences from controls compared to normoxia (Fig. 2A and B). Since myotubes rely predominantly on OXPHOS, DUX4-induced interference with hypoxic adaptation should render FSHD myotubes more vulnerable to redox imbalances than FSHD myoblasts. We thus compared ROS levels of control versus FSHD myoblasts and myotubes between normoxia and hypoxia. Hypoxia did not elicit differential changes in ROS levels in FSHD and control myoblasts, but myotubes displayed a larger increase in ROS levels compared to control myotubes when differentiated in hypoxia (Fig. 8C). In general, ROS levels in both hypoxic control and FSHD myotubes increased dramatically (approximately two-fold in controls) compared to normoxia, but we observed a disproportionate increase in hypoxic FSHD myotubes. The concomitant increase of ΔΨm in hypoxic FSHD myotubes (Fig. 8A) again suggests that this differential increase is caused by altered mitochondrial ROS metabolism. Notably, hypoxia consistently aggravated the hypotrophic FSHD myotube phenotype observed in normoxia in all three patient-derived models, whereas control myotubes did not generally show any gross morphological impairment of differentiation in hypoxia (Fig. 8D and E). Likewise, control myotubes differentiated in normoxia under exogenous oxidative stress (400 μM H_2O_2) or chemically-induced hypoxia (100 μM $CoCl_2$) displayed a hypotrophic myotube phenotype similar to that of FSHD myotubes (Fig. S5). These observations strongly suggest that failure of FSHD myotubes to adapt their metabolism to hypoxia to maintain redox control and prevent oxidative stress/damage is the driving mechanism underlying myotube hypotrophy.

2.7. Mitochondria-targeted antioxidants efficiently rescue hallmarks of FSHD

Conventional, non-targeted antioxidant treatment can rescue aspects of FSHD pathology *in vitro* [48,57,76] and *in vivo* [59,60], although with only moderate therapeutic efficiency. In addition, antioxidant rescue studies *in vitro* have only been performed under ambient O_2 levels, so potential therapeutic effects on metabolic switching under low O_2 availability are unknown. Having identified that mitoROS production by dysfunctional mitochondria upstream of oxidative stress disturbs FSHD myogenesis, specifically in hypoxia, we tested whether a more targeted antioxidant approach could more effectively rescue FSHD pathological hallmarks in hypoxic myotubes.

We selected 3 well-established antioxidant compounds with different modes of action and subcellular localisation: Vitamin C (VitC), a classic non-targeted antioxidant which is mostly retained in the cytoplasm; Coenzyme Q10 (CoQ10; ubiquinone-10), a lipophilic compound naturally involved in the mitochondrial ETC that can thus localise, to some extent, to mitochondria as well as other membranes; and mitoTEMPO, a mitochondria-targeted SOD-mimetic that accumulates several hundred-fold in mitochondria compared to cytoplasm due to its lipophilic cationic triphenylphosphonium moiety.

Initially, we tested for their ability to reduce ROS levels and ΔΨm after DUX4 induction in hypoxic iDUX4 myotubes under 1% O_2, which produced the strongest morphological and redox phenotypes. VitC, CoQ10 and mitoTEMPO all reduced general ROS levels, with VitC and mitoTEMPO showing highest efficiency and almost identical reduction (Fig. 9A). This further emphasizes that mitoROS could be the primary trigger of oxidative stress, as ROS can leave the mitochondria in the form of H_2O_2 after dismutation by SOD, which would enable subsequent detoxification by cytoplasmic antioxidants like VitC. Notably though, only mitoTEMPO could reduce ΔΨm in response to DUX4 expression (Fig. 9B), demonstrating that (i) mitochondrial membrane polarisation is at least in part mediated by redox changes elicited by mitoROS and (ii) mitochondria-targeted antioxidant treatment may directly alleviate DUX4-induced mitochondrial dysfunction. Since mitoROS are a prerequisite for hypoxia signalling activation, only antioxidants capable of entering the mitochondria (mitoTEMPO and, to a much lesser extent, CoQ10) reduced iDUX4 myotube hypoxia (Fig. 9C). Interestingly, only mitoTEMPO was able to improve metabolic activity in DUX4 expressing myotubes, with VitC showing a detrimental effect, possibly due to pro-oxidant mechanisms (Fig. 9D). Importantly, all three compounds were able to rescue DUX4-induced myotube hypotrophy (Fig. 9E).

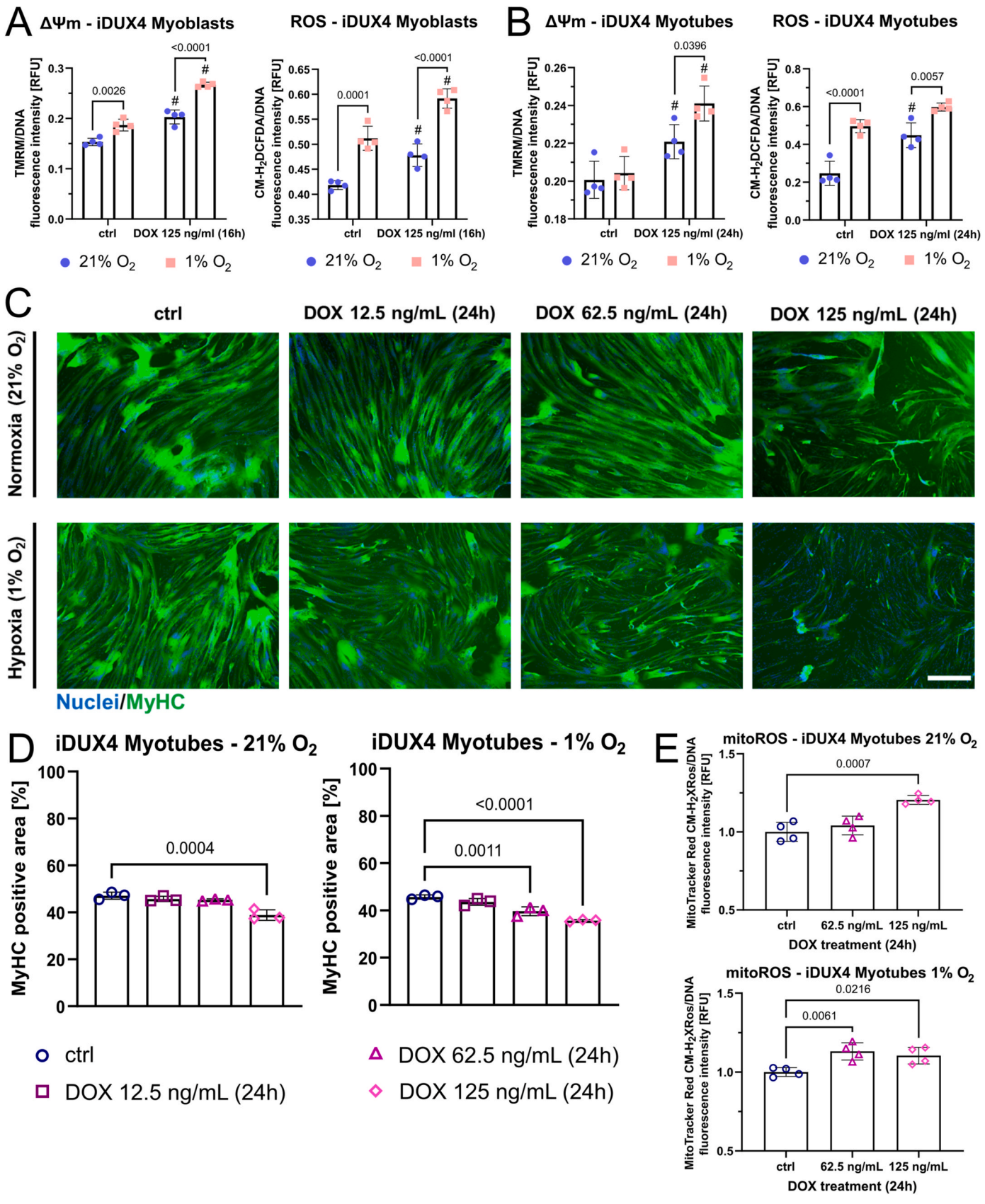

(caption on next page)

Fig. 7. ***DUX4-induced mitochondrial dysfunction impairs myogenesis in hypoxia through aggravation of oxidative stress.*** **(A, B)** Hypoxia under 1% O_2 increases oxidative stress in non DUX4-induced iDUX4 myoblasts and myotubes. DUX4 expression (DOX 125 ng/mL for 24 h) increases ΔΨm (assessed by measuring TMRM fluorescence) and ROS levels (assessed by CM-H_2DCFDA fluorescence) regardless of O_2 tension (# denotes statistical significance between DUX4 induction at given O_2 tension and the respective non-induced control), with ΔΨm and ROS levels even further increasing in hypoxia. **(C, D)** Titration of the DUX4-inducer DOX (for 24 h at variable amounts) in iDUX4 myotubes demonstrates that lower DUX4 levels are needed to produce a hypotrophic myotube phenotype in hypoxia compared to normoxia, as assessed by quantitation of the MyHC (green) containing area from immunofluorescence micrographs (scale bar represents 500 μm). **(E)** DUX4 expressing myotubes are characterised by significantly elevated mitochondrial ROS levels (assessed by MitoTracker® Red CM-H_2XROS fluorescence) at the minimal DOX concentration needed to elicit a hypotrophic myotube phenotype in hypoxia versus normoxia. Data is mean ± s.d. from 3 to 4 wells each from a representative experiment with *p* values as indicated. (For interpretation of the references to colour in this figure legend, the reader is referred to the Web version of this article.)

We also tested these three antioxidants in patient-derived FSHD myotubes in hypoxia. All compounds reduced ROS levels with similar efficiency, but mitoTEMPO again was most efficient in reducing FSHD myotube ΔΨm and hypoxia, and improving metabolic activity (Fig. 10A and Fig. S6). Notably, all three antioxidant compounds rescued FSHD myotube hypotrophy in hypoxia (Fig. 10B and C), demonstrating that targeting of redox-sensitive FSHD pathomechanisms has direct and beneficial effects on FSHD myogenesis under increased oxidative stress.

Our analysis demonstrates that the efficiency of a given antioxidant compound in rescuing redox-sensitive FSHD pathomechanisms correlates with its ability to localise to mitochondria.

3. Discussion

This work for the first time provides a pathomechanistic model integrating two previously identified but under-studied central pathologic hallmarks of FSHD: mitochondrial dysfunction and disturbed hypoxia signalling. We identify that complex I-linked mitochondrial respiration is strongly and uniquely impaired in FSHD patient-derived muscle biopsies at the transcriptomic level, with robust and significant inverse correlation between disease severity and mitochondrial protein-coding gene expression. We further demonstrate at the functional level that complex I-linked respiration is specifically affected by DUX4, disturbing the molecular response to hypoxia through HIF1α when DUX4 expressing cells are cultured in environmental hypoxia. We pinpoint involvement of enhanced mitoROS generation from the ETC, driven by ΔΨm, and show that mitochondria-targeted antioxidants efficiently rescue FSHD phenotypes in iDUX4 and patient-derived models, especially when impaired metabolic adaptation to hypoxia increases oxidative stress in FSHD myotubes. In summary, our findings strongly suggest that DUX4 causes widespread metabolic stress, likely through mechanisms involving DUX4-induced redox perturbations triggering mitochondrial oxidative modifications and damage, and through more widespread transcriptional changes elicited by DUX4 in the nuclear genome (Fig. 11).

Supraphysiological DUX4 levels in DUX4-inducible muscle cell models might lead to overestimation of DUX4 toxicity, as even low to moderate DOX concentrations already yield DUX4 levels much higher than found in FSHD patient-derived cell models and biopsies, where DUX4 is notoriously difficult to even detect [77]. We thus investigated redox changes in patient-derived models of FSHD as well as the LHCN-iDUX4 model, and found that changes in cellular ROS metabolism are remarkably consistent between both models, highlighting the central involvement of DUX4 in metabolic stress in FSHD. Specifically, FSHD mitochondria are characterised by hyperpolarised membranes, evident as a steady-state increase of ΔΨm in FSHD myoblasts and myotubes. Similarly, DUX4 expression elevates ΔΨm in a dose-dependent manner. Since the relationship between ΔΨm and mitoROS production is exponential [78], even a small but chronic increase in ΔΨm can trigger high $O_2^{\bullet-}$ production through drastically increased electron leakage from the respiratory chain. The notion that DUX4-induced changes in ΔΨm precede elevated ROS levels and subsequent apoptosis (marked by a gradual depolarisation of the mitochondrial membrane) strongly suggests that the majority of ROS in FSHD stem from the respiratory chain, placing mitochondrial dysfunction upstream of oxidative damage.

Lipid peroxidation has been found in FSHD patient muscles [46] and our results are in line with recent work demonstrating that even low level DUX4 expression can trigger mitochondrial lipid peroxidation [61]. Further, membrane repair deficits have been identified in FSHD myoblasts and DUX4 expressing murine myofibres *ex vivo*, which can be alleviated through antioxidant treatment [76]. Membrane lipid peroxidation is a comparably specific oxidative mechanism but it is unclear what RONS are involved, as is how more general oxidative/nitrosative protein modifications affect muscle function in FSHD. Central involvement of hydroxyl ($^{\bullet}$OH) radicals and peroxynitrite ($ONOO^-$) in lipid peroxidation is well established [79,80], the latter arising from rapid reaction between NO• and $O_2^{\bullet-}$. Since our transcriptomic analysis also identified impaired nitrogen metabolism in FSHD muscle, elevated mitoROS production could result in increased $ONOO^-$ formation, thereby eliciting (mitochondrial) lipid peroxidation at the expense of NO• bioavailability. Kinetics and compartmentalisation of interplay between $O_2^{\bullet-}$ and NO• are thus critical in transforming physiological regulatory effects of NO• to cytotoxic mechanisms through oxidative damage. Of note, NO• also participates in redox signalling pathways upstream of PGC1α-mediated mitochondrial biogenesis and turnover, which we have previously found dynamically repressed in FSHD myogenesis [52]. In this respect, the versatile role of NO• in redox-regulation of skeletal muscle function through direct modulation of mitochondrial respiration and signalling [81–83], hypoxia response [84,85] and apoptosis [86,87] prompts research into the pathomechanistic contribution of perturbations of the nitrosative system through mitoROS in FSHD.

Having identified mitochondrial membrane polarisation and mitoROS at the core of DUX4-induced redox perturbance, our respirometric analysis revealed that mitochondrial dysfunction in response to DUX4 expression is uniquely conferred through complex I, a known major source of mitoROS production [88]. Although several other sites of $O_2^{\bullet-}$ production have been identified in mitochondria, complex I, alongside complex III, is considered the main driver of ROS production from the ETC [89], specifically at high pmf/ΔΨm. Although it is unclear to what extent individual ROS generating systems in the mitochondria contribute to oxidative stress in FSHD, as complex II-linked respiration was largely unaffected by DUX4, this suggests complex I as major source. Furthermore, as far as the substrate entry points into the ETC are concerned, complex I contributes to generation of ΔΨm while complex II does not under normal circumstances, linking mitochondrial membrane hyperpolarisation with altered complex I function. Chronic complex I inhibition causes mitochondrial membrane hyperpolarisation due to concomitant inhibition of complex V [90]. Hyperpolarisation elevates mitoROS levels and induces mitoROS-mediated mitochondrial apoptosis and aging [91–93]. Reverse electron transport (RET) could be the reason for mitochondrial membrane hyperpolarisation and enhanced $O_2^{\bullet-}$ production by complex I, a mechanism previously shown during

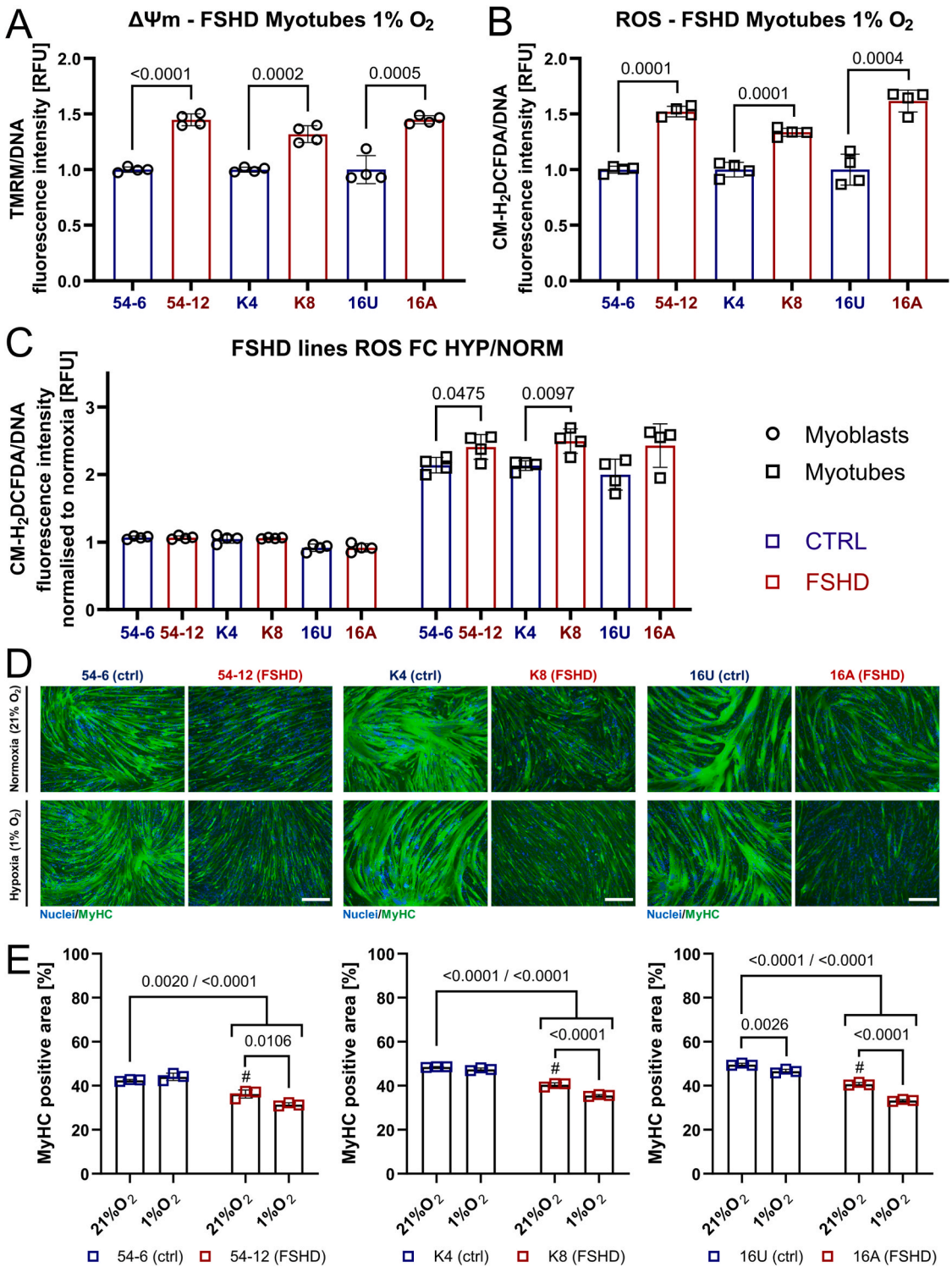

Fig. 8. ***FSHD myogenesis is particularly susceptible to hypoxia-induced oxidative stress.*** **(A, B)** FSHD patient myotubes (54-6 ctrl/54-12 FSHD; K4 ctrl/K8 FSHD; 16U ctrl/16A FSHD) maintain significantly elevated ΔΨm (assessed by measuring TMRM fluorescence) and ROS levels (assessed by CM-H_2DCFDA fluorescence) in hypoxia under 1% O_2 compared to isogenic/sibling controls, but differences are more pronounced than in normoxia (compare to Fig. 2A and B). **(C)** Hypoxia increases ROS levels in FSHD patient myotubes disproportionally compared to controls, which is not observed in FSHD myoblasts (FC HYP/NORM: fold change in hypoxic myoblasts/myotubes compared to their respective normoxic controls). **(D)** FSHD myotubes differentiated in hypoxia fail to properly adapt metabolism to low O_2 availability, resulting in an aggravated hypotrophic phenotype as shown by immunolabelling for MyHC (green), with a nuclear HOECHST33342 counterstain (blue). Hypoxic control myotubes are not affected (scale bar represents 250 μm). **(E)** Quantitation of MyHC-containing area as readout for myotube hypotrophy from immunofluorescence micrographs (# denotes statistical significance between MyHC-positive area of normoxic FSHD myotubes and their hypoxic controls). Data is mean ± s.d. from 3 to 4 wells each from a representative experiment with *p* values as indicated. (For interpretation of the references to colour in this figure legend, the reader is referred to the Web version of this article.)

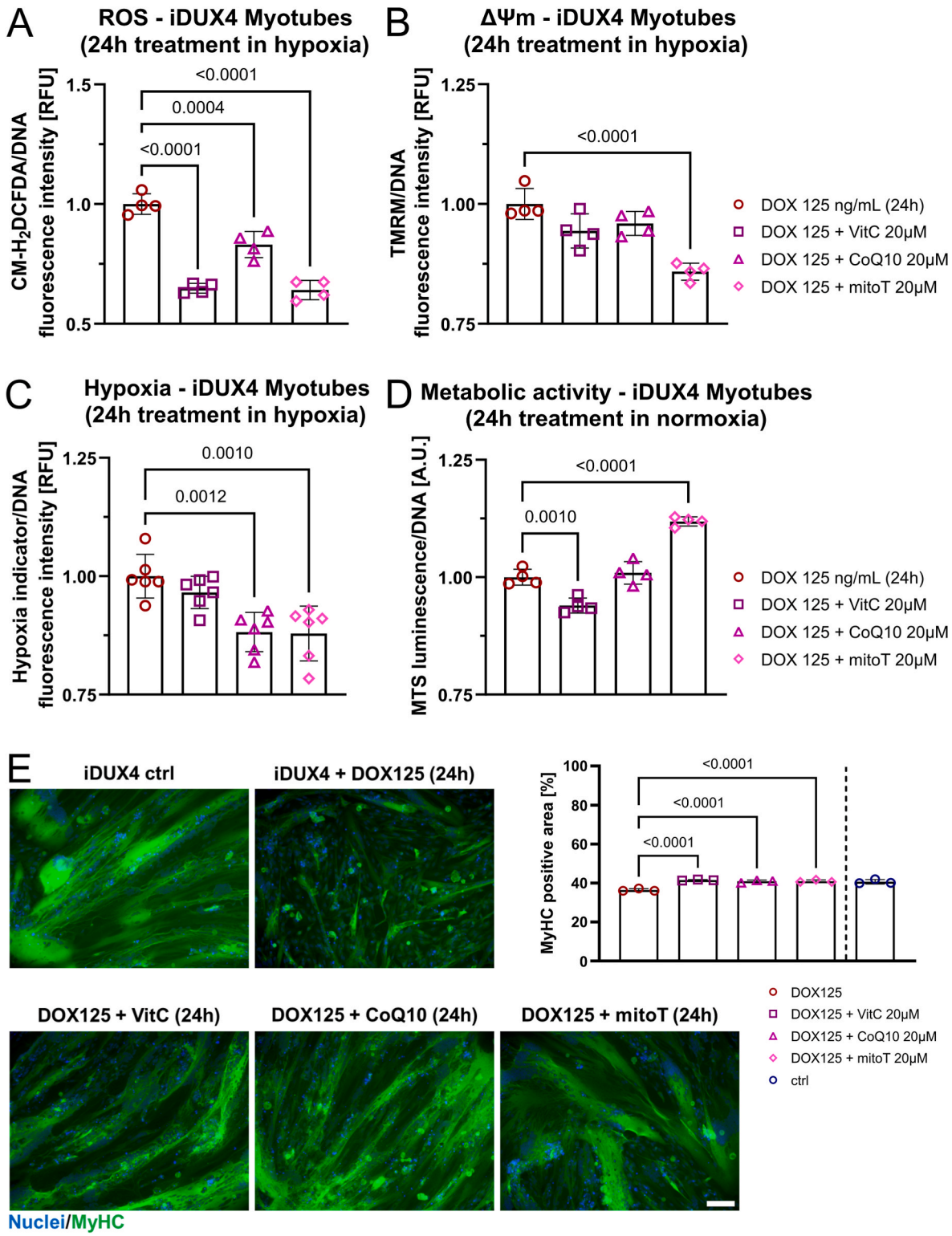

Fig. 9. ***Mitochondria-targeted antioxidants more efficiently rescue DUX4-induced metabolic/hypoxic stress than conventional antioxidants.*** **(A)** Treatment of hypoxic iDUX4 myotubes (induced with 125 ng/mL DOX for 24 h under 1% O2) with mitochondria-targeted mitoTempo (mitoT) or conventional CoQ10 or VitC antioxidants effectively reduces ROS levels (assessed by CM-H_2DCFDA fluorescence) in response to DUX4, (**B**) but only mitoTempo normalises ΔΨm (assessed by measuring TMRM fluorescence), and (**C**) reduces hypoxia (measured using Image-IT™ Green Hypoxia Reagent fluorescence). (**D**) Only mitoTempo restores metabolic activity in normoxic myotubes (induced with 125 ng/mL DOX for 24 h under 21% O2), as measured using the luminescence RealTime-Glo™ MT Cell Viability assay with normalisation to DNA content). **(E)** mitoTempo phenotypically rescues DUX4 expressing iDUX4 myotubes in hypoxia with similar efficiency as non-targeted CoQ10 and VitC, emphasising central involvement of mitoROS as source of metabolic/hypoxic stress. Representative immunofluorescence micrographs are shown (scale bar represents 100 μm), as is quantitation of the MyHC-containing area (green) for each treatment group. Data is mean ± s.d. from 3 to 6 wells each from a representative experiment with *p* values as indicated. (For interpretation of the references to colour in this figure legend, the reader is referred to the Web version of this article.)

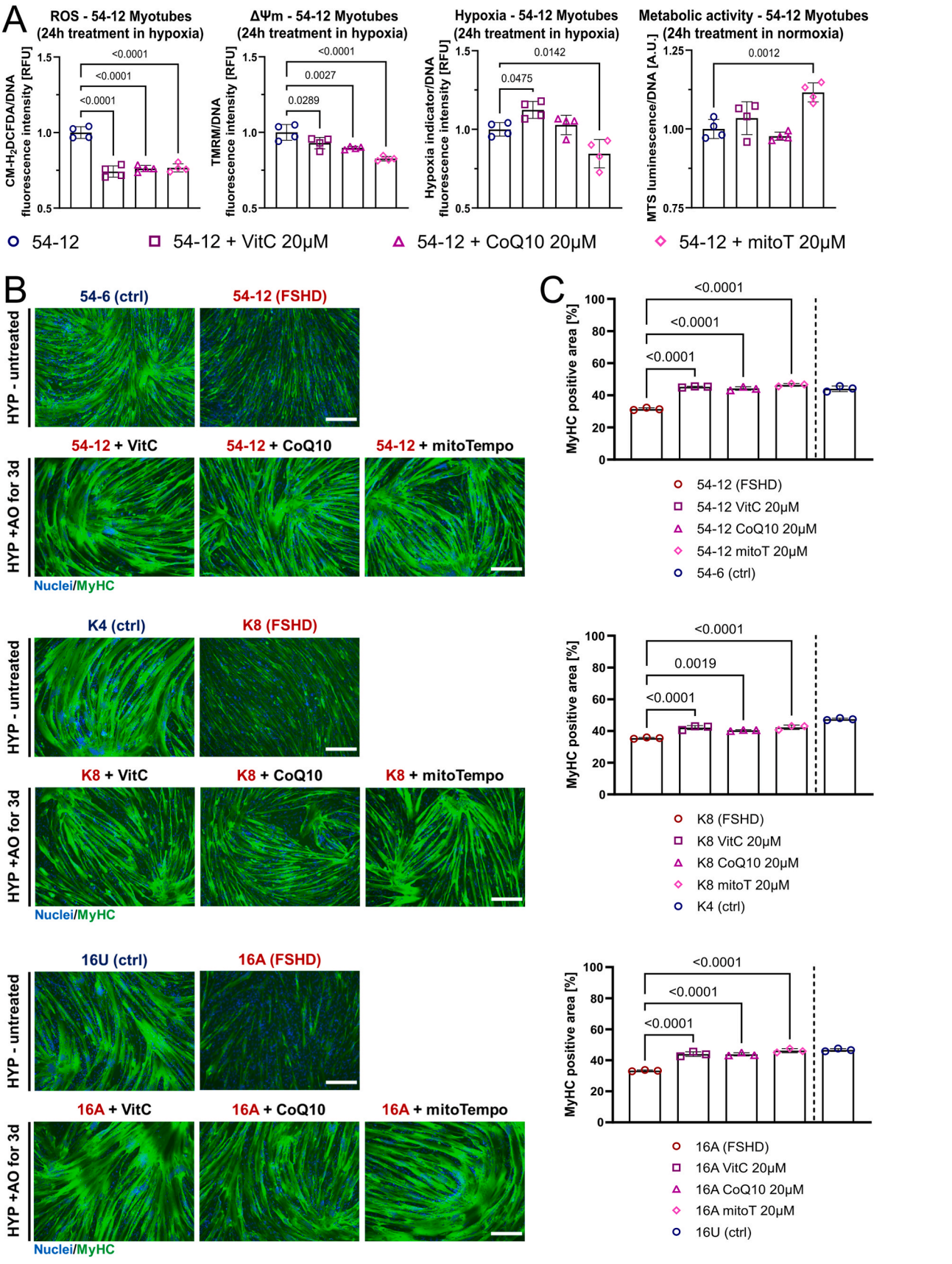

(caption on next page)

Fig. 10. ***Mitochondria-targeted antioxidants alleviate oxidative stress and rescue aggravated FSHD myotube hypotrophy in hypoxia.*** **(A)** mitoTempo (mitoT), CoQ10 and VitC demonstrate comparable efficiency in reducing ROS levels (assessed by CM-H_2DCFDA fluorescence) in hypoxic FSHD (54-12) patient myotubes maintained in 1% O_2, but mitoTempo shows highest ability to normalise ΔΨm (assessed by measuring TMRM fluorescence) and reduce hypoxia (measured using Image-IT™ Green Hypoxia Reagent fluorescence). Only mitoTempo restores metabolic activity (measured using the luminescence RealTime-Glo™ MT Cell Viability assay with normalisation to DNA content) in normoxic FSHD (54-12) myotubes maintained in 21% O_2. **(B)** mitoTempo treatment phenotypically rescues FSHD myotube hypotrophy in hypoxia in 3 independent patient lines with similar efficiency as non-targeted CoQ10 and VitC. Representative immunofluorescence micrographs are shown of immunolabelling for MyHC (green), with a nuclear HOECHST33342 (blue) counterstain [images of hypoxic controls from Fig. 8, are part of this experiment (scale bar represents 250 μm)]. HYP: hypoxia (1% O_2), AO: antioxidant treatment. **(C)** Quantitation of the MyHC-containing area for each antioxidant treatment group compared to untreated FSHD myotubes (*K8 CoQ10 data from a separate experiment, with given *p* value to that control). Untreated isogenic/sibling control included for comparison. Data is mean ± s.d. from 3 to 4 wells each from a representative experiment with *p* values as indicated. (For interpretation of the references to colour in this figure legend, the reader is referred to the Web version of this article.)

complex II-dependent succinate-driven respiration [94]. In addition, F_0F_1-ATPase contributes to generation of ΔΨm when RET occurs to maintain pmf on account of the hydrolysis of cytoplasmic ATP [95]. Our transcriptomic analysis from patient biopsies strongly supports complex I as the main trigger of mitochondrial dysfunction, identifying mitochondrial complex I assembly as the top enriched GOBP, along with strong enrichment for genes involved in mitochondrial gene expression, energy metabolism and, more general, respiratory chain complex assembly. Notably, we also identified robust transcriptional downregulation of all 13 protein-coding genes in the mitochondrial genome (of which 6 encode complex I subunits), indicating that mitochondrial gene expression is severely challenged by DUX4. It remains to be determined whether this is a consequence of DUX4-induced oxidative mtDNA damage and thus gradual mtDNA instability, perturbance of the coordination between nuclear and mitochondrial gene expression during mitochondrial remodelling and biogenesis, and/or general reduction of mtDNA content. Interestingly, our GOBP analysis also revealed a strong link between pathways of mitochondrial (dys)function and nitrogen metabolism, with a considerable number of genes shared across both GO terms.

We observed a direct correlation between respiration and cellular hypoxia. DUX4 expression in myoblasts elicited a state resembling metabolic hypoxia [96], where decreased complex I-linked OXPHOS correlated with a decrease in the percentage of HIF1α-positive nuclei, suggesting altered hypoxia sensing/signalling. In myotubes, DUX4 had the opposite effect, with higher O_2 consumption through increased complex I-linked OXPHOS further enhancing cellular hypoxia and HIF1α nuclear stabilisation. This correlation suggests that redistribution of O_2 from the respiratory chain towards other O_2-sensitive circuits (such as HIF1α activation) is a primary mechanism by which mitochondrial dysfunction affects hypoxia signalling in FSHD. Observed differences in OXPHOS between myoblasts and myotubes emphasise the importance of looking at DUX4-induced metabolic and redox changes over various developmental stages of myogenesis, since myoblasts mainly rely on glycolytic metabolism while *in vitro* terminally differentiated myotubes switch to OXPHOS as main energy source [97–100]. This is highlighted by significant increase in mitochondrial mass and enzyme activity shortly after the onset of myogenic differentiation, and mitochondria have been identified as potent regulators of developmental and regenerative myogenesis [101]. However, the gradual switch from glycolytic to oxidative metabolism also renders myotubes a redox biological system quite different from myoblasts, as myotubes are much better equipped to deal with oxidative stress as a natural and inevitable by-product of the bioenergetically more efficient OXPHOS. This difference may explain the increased susceptibility of FSHD myoblasts to oxidative stress compared to FSHD myotubes [40]. In this respect, the DOX concentrations used for respirometric analysis likely triggered much higher levels of oxidative stress/damage in iDUX4 myoblasts than in myotubes. Much higher concentrations of DOX were needed to trigger significantly elevated ROS levels in myotubes compared to myoblasts, and DOX treatment of myotubes with 62.5 ng/mL for 24 h only yielded around 5% DUX4-positive myonuclei (as opposed to around 45% DUX4-positive nuclei in myoblasts), which did not elicit a morphological myotube phenotype in normoxia. Nevertheless, pro-apoptotic iDUX4 myoblasts after 16 h DOX treatment were marked by reduced complex I-linked OXPHOS and LEAK respiration, indicative of putative $ONOO^-$-mediated impairment of mitochondrial membrane integrity, of complex I itself through irreversible S-nitrosylation, and, possibly, of mitochondrial transport proteins. Whether DUX4 initially affects ΔΨm and OXPHOS through perturbance of the mitochondrial transmembrane systems shuttling ions and metabolites, or directly through generation of mitochondrial oxidative stress, which then causes mitochondrial dysfunction, remains to be elucidated. A more thorough, kinetic respirometric analysis of DUX4-induced effects on OXPHOS will be needed to identify early versus late effects on mitochondrial (dys)function, specifically in myotubes where increased complex I-linked respiration could be an early event before the oxidative stress response is overwhelmed and complex I becomes irreversibly inhibited, as observed in the more oxidative stress-sensitive myoblasts.

Given that changes in OXPHOS directly affect cellular O_2 consumption and are thus inevitably linked to hypoxia signalling activity, any impairment of mitochondrial function will impinge on the ability of cells to metabolically adapt to environmental hypoxia. Even though the relationship between hypoxia in terms of HIF1α activation and mitoROS generation and its physiological significance remains controversial, there is accumulating evidence that myogenic cells produce higher amounts of ROS from the respiratory chain under hypoxic conditions [75,102,103]. We found that hypoxic culture increased ROS levels in non-induced iDUX4 myoblasts/myotubes, which were further increased by DUX4. Likewise, lower concentrations of DOX were sufficient to impair myotube formation in hypoxia compared to normoxia.

Since hypoxia did not overtly affect control myogenesis in non-induced cells, we hypothesise that DUX4 further increases hypoxia-induced oxidative stress through interference with hypoxic metabolic adaptation via HIF1α. mitoROS are a prerequisite for HIF1α activation [104,105], and we found significantly elevated mitoROS levels in DOX treatment groups that produced a hypotrophic myotube phenotype. It is thus likely that, apart from O_2 redistribution (through increased complex I-linked OXPHOS), DUX4 also causes enhanced mitoROS production from complex I to further disturb the response to hypoxia in myotubes by interference with metabolic adaptation through over-stimulation of HIF1α. Although the relation between hypoxia and ΔΨm is not completely understood, further elevation of ΔΨm by DUX4 in hypoxia (compared to normoxia) is probably the cause for enhanced oxidative stress in hypoxic myotubes through mitoROS. Similar to the iDUX4 model, FSHD patient-derived myotubes maintain higher ΔΨm and ROS levels in hypoxia, the latter increasing disproportionally in hypoxic FSHD myotubes compared to normoxia. Hence, FSHD myotubes displayed aggravated hypotrophy when differentiated in hypoxia. Notably, this was not observed in FSHD myoblasts, where FSHD clones exhibit higher ROS levels in hypoxia (data not shown) and normoxia, but hypoxia did not increase ROS levels differentially. This suggests that two factors, oxygen concentration and ΔΨm, predominantly regulate ROS-dependent HIF1α stabilisation in FSHD myotubes.

Consistency between the results obtained in hypoxic DUX4 expressing and FSHD myotubes strengthens our observations and strongly suggests central involvement of DUX4 as the trigger of

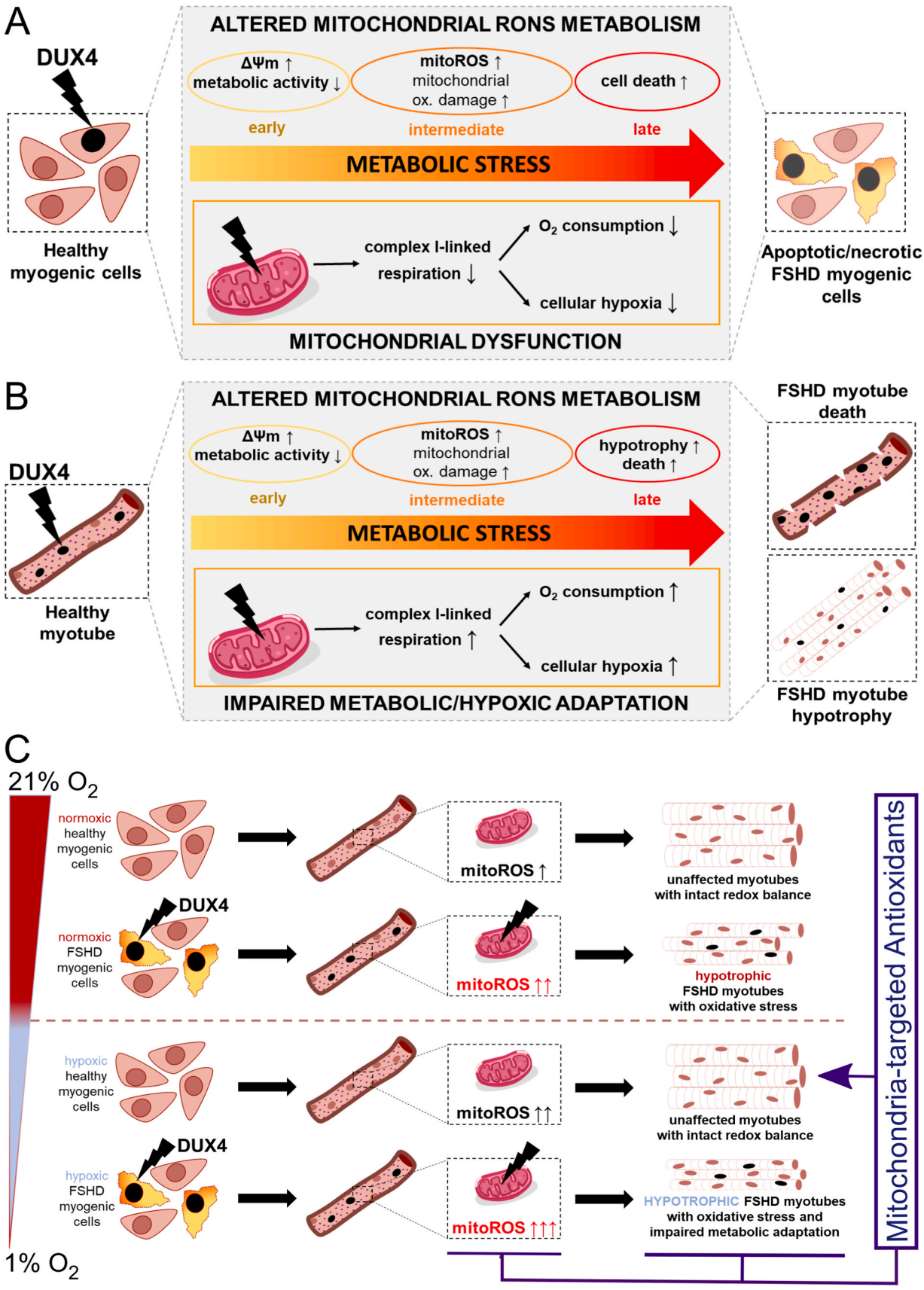

(caption on next page)

Fig. 11. ***Mechanisms of metabolic stress generation in FSHD.*** **(A)** DUX4 triggers metabolic stress in myoblasts through alterations in mitochondrial ROS metabolism and function. Hyperpolarisation of the mitochondrial membrane is an early event in response to DUX4, followed by mitochondrial oxidative damage through enhanced mitoROS formation from the respiratory chain. Mitochondrial dysfunction is conferred through reduced complex I-linked respiration, affecting hypoxia signalling through redistribution of O_2. **(B)** DUX4 also triggers oxidative damage and altered mitochondrial ROS metabolism driven by high ΔΨm in myotubes, resulting in myotube hypotrophy and apoptosis. Increased O_2 consumption via complex I, and enhanced mitoROS formation, both trigger hypoxia in myotubes. **(C)** DUX4-induced redox changes challenge mitochondrial health and function through altered ROS metabolism, and thus interfere with metabolic adaptation to environmental hypoxia. Enhanced mitoROS formation triggered by DUX4 in normoxic myotubes is further increased in hypoxia, concomitant with aggravation of the hypotrophic myotube phenotype. Notably, FSHD myotubes are particularly sensitive to hypoxia-induced metabolic/oxidative stress, whereas control myotubes adapt their metabolism to prevent oxidative stress through excess mitoROS. Given that mitoROS-induced oxidative stress is a main driver of myotube hypotrophy in hypoxia, mitochondria-targeted antioxidants alleviate FSHD phenotypes more efficiently than conventional non-targeted antioxidants. Thus, affected mitochondria in FSHD are a primary trigger of muscle loss associated with the disease, specifically when metabolic adaptation to varying O_2 availability is required. These phenotypes occur in both FSHD patient-derived and iDUX4 human cells.

oxidative stress and hypoxia sensitivity. Involvement of DUX4-induced oxidative stress as a negative regulator of FSHD myogenesis has mainly been shown in DUX4 overexpression systems, where antioxidants can alleviate myopathic phenotypes [32,48,76], but rarely in FSHD patient-derived cellular models, marked by much lower and sporadic DUX4 expression. In addition, conventional, non-targeted antioxidants have been investigated in all but one study [61]. To pinpoint involvement of mitoROS and hypoxia in FSHD pathogenesis, we used antioxidant compounds with different abilities to localise to mitochondria. VitC, CoQ10, mitoTEMPO all reduced ROS levels in DUX4 expressing hypoxic myotubes and rescued the hypotrophic myotube phenotype with comparable efficiency, but only mitochondria-targeted mitoTEMPO reduced ΔΨm and hypoxia, while restoring metabolic activity. These findings suggest that (i) the respiratory chain is a major contributor to oxidative stress through mitoROS (specifically when metabolic switching is required in response to hypoxia), (ii) mitoROS initially released into the mitochondrial matrix or intermembrane space eventually escape into the cytoplasm as H_2O_2 to further interfere with the cellular redox balance, and (iii) mitoROS are involved in over-stimulation of HIF1α in DUX4 expressing myotubes. Likewise, antioxidant treatment rescued the hypotrophic phenotype of hypoxic FSHD myotubes in three separate patient-derived myoblast lines, where FSHD myotubes had shown increased sensitivity to hypoxia. Notably, mitoTEMPO was most efficient in normalising ΔΨm, reducing hypoxia and restoring metabolic activity through its ability to enrich within mitochondria, yet no difference in the ability of the antioxidants to morphologically rescue FSHD myogenesis was observed, further underscoring that oxidative stress in FSHD stems predominantly from mitoROS.

In summary, we have identified mitochondrial dysfunction followed by elevated generation of mitoROS as a primary mechanism by which DUX4 causes oxidative stress in FSHD (Fig. 11). We provide a link between the redox biological changes elicited through disturbed ROS metabolism and hypoxia sensitivity, and show complex I dysfunction with enhanced mitoROS production from the respiratory chain as a main trigger of DUX4-mediated pathogenesis. We further demonstrate that mitochondria-targeted antioxidants are more effective in alleviating aspects of disturbed myotube metabolism compared to conventional antioxidants, highlighting involvement of the respiratory chain as a source of ROS. Given the moderate clinical outcomes in FSHD patients seen in clinical trials employing non-targeted antioxidants [60,106], mitochondria-targeted compounds should be a more efficient approach, as they target ROS directly at the site of generation and require much lower concentrations to be effective *in vivo* while interfering less with physiologically important redox pathways [107]. Indeed, mitochondria-targeted antioxidants have been proven safe in humans [108], with beneficial effects in phase II clinical trials for hepatitis C [109] and dry eye treatment [110]. A limitation of this study is that we did not compare in detail the pharmacological effects of the tested antioxidants, however, mitochondria-targeted antioxidants are generally efficient in much lower concentrations than untargeted ones.

Mitochondria-targeted antioxidants will also be useful to elucidate the mechanistic role of disturbed mitochondrial ROS metabolism in FSHD pathogenesis. Of significance, two prominent extra-muscular features of FSHD, retinal telangiectasia and sensorineural hearing loss, have also been linked with oxidative stress and mitochondrial dysfunction [111,112]. Both retina and cochlea are characterised by high metabolic activity, and, specifically, the central involvement of OXPHOS deficits in the pathophysiology of hearing loss is well characterised [113]. While the beneficial effects of conventional antioxidants in treatment of hearing loss remain controversial [114], mitochondria-targeted antioxidants have yielded promising results in animal studies [115].

It is crucial to now identify how DUX4 challenges cellular redox pathways to understand the extent of the metabolic stresses in FSHD. Deeper understanding of OXPHOS-related pathomechanisms will not only inform novel therapeutics such as mitochondria-targeted antioxidants, Szeto-Schiller (SS) peptides or mild uncouplers [116,117], but will likely also reveal novel aspects of FSHD aetiology. DUX4 affects more than 200 genes "indirectly" by oxidative stress in normoxic myoblasts [61]. Given discrepancies between the available transcriptomic and proteomic data sets [118], investigating DUX4-induced transcriptional changes will not allow conclusions regarding the FSHD metabolome. Dynamic transcriptomic-metabolomic analyses of FSHD myogenesis under O_2 tensions to model physioxia and hypoxia are needed to find novel pathomechanisms related to metabolic adaptation undetectable in normoxia. This will not only decipher mechanisms of metabolic stress related to hypoxia, but will also identify whether the redox-sensitive core oxidative metabolic pathways providing substrates for OXPHOS are uniquely affected, in addition to the mitochondrial respiratory chain. Since FSHD patients show signs of both muscular and systemic oxidative stress/damage, evaluation of mechanisms described here in non-myogenic FSHD models will be useful to investigate how aspects of DUX4-induced redox perturbance affect cell and tissue function in these models.

4. Materials and methods

4.1. Transcriptomic analyses

For differential expression (DE) analysis, RNA-Seq data (gene counts) of muscle biopsies from 6 severely affected FSHD patients and 9 unaffected individuals were obtained from GSE115650 [62]. Data processing was performed as recently described [119]. Briefly, filtering for lowly expressed genes (CPM <1) and further biotype filtering was performed in R with the Bioconductor packages NOISeq [120] and biomaRt [121] to remove highly expressed mitochondrial and ribosomal RNA. DE analysis was performed using the Bioconductor package edgeR [122]. Specifically, a negative binomial generalized log-linear model (glmfit) was fitted to the read counts and the likelihood ratio test (glmLRT) was conducted for each comparison of interest. The Benjamini-Hochberg false discovery rate (FDR) cut-off was set at 0.05. The versions of all relevant Bioconductor packages were compatible with R v3.5.3.

Heatmap depicting expression levels of the 887 unique genes listed in all GOs referring to superclusters Mitochondrial Activity & Organisation, Response to oxidative stress and oxygen levels and metabolism of

nitrogen compound, was generated using Morpheus (https://software.broadinstitute.org/morpheus/) applying the function "One plus Log2" followed by hierarchical clustering. Heatmap depicting expression of mitochondrial protein-coding genes in FSHD myotubes was generated similarly in Morpheus, which was also used to perform hierarchical clustering to evaluate the ability of the expression pattern of 13 mitochondrial genes to separate between FSHD and control transcriptomes. Heatmap displaying expression of mitochondrial protein-coding genes and DUX4 target genes referring to patients of groups 1, 2,3 and 4 (group 1 = lowest severity, group 4 = highest severity, as stratified in Ref. [62]) was generated using unfiltered CPM values from GSE115650 [62]. For each gene, the average expression value across all patients within the same disease group was calculated, and z-score transformed to normalise across all disease groups.

For pathway and gene set analysis, we used WebGStalt (www.webgestalt.org) to assess gene ontology terms that showed significant enrichment in the list of DEG (Overrepresentation Enrichment Analysis). The enrichment for each GO Biological Process (GOBP) term was considered statistically significant if the adjusted p-value (FDR) was lower than 0.05. Only the top 30 GOs are reported in Fig. 1. Cytoscape v. 3.7.2 [123] was used to visualise relevant biological networks of enriched GOBPs, together with EnrichmentMap and AutoAnnotate applications. Several layout parameters were tuned to achieve the current Cytoscape visualization.

4.2. Cell culture and myogenic differentiation

The three immortalised FSHD patient-derived cellular models were the isogenic '54' series derived from the biceps of a male mosaic FSHD1 patient [124], where 54-6 (13 D4Z4 repeats) is the uncontracted control clone and 54-12 (3 D4Z4 repeats) the contracted FSHD clone; the isogenic 'K' (KM271FSH44TA) series from the tibialis anterior of a mosaic FSHD1 patient, with 44-4 (K4) the uncontracted control and 44-8 (K8) the D4Z4-contracted FSHD clone; and the '16' series, a sibling-matched immortalised model derived from biceps muscle [125], where 16A is the D4Z4 contracted FSHD line and 16U the uncontracted control line from a first-degree relative. The inducible DUX4 myoblast line (iDUX4) was LHCN-M2-iDUX, on the human LHCN-M2 myoblast background [126]. DUX4 expression was induced by doxycycline (DOX; Sigma Aldrich, Dorset, UK).

Human myoblast lines were cultured in Skeletal Muscle Cell Growth Medium (Promocell, Heidelberg, Germany) supplemented with 20% foetal bovine serum (FBS; ThermoFisher Scientific, MA, USA), 50 μg/mL fetuin (bovine), 10 ng/mL epidermal growth factor (recombinant human), 1 ng/mL basic fibroblast growth factor (recombinant human), 10 μg/mL insulin (recombinant human), 0.4 μg/mL dexamethasone (all added as PromoCell SupplementMix) and 50 μg/mL gentamycin (Sigma Aldrich) in a humidified incubator at 37 °C with 5% CO_2. Myoblast lines were kept subconfluent in routine culture, and passaged at maximum 70% confluency.

To induce differentiation, myoblasts were washed twice with phosphate buffered saline (PBS) and placed in Dulbecco's Modified Eagle Medium (DMEM) GlutaMax (ThermoFisher Scientific) supplemented with 0.5% FBS, 10 μg/mL recombinant human insulin (Sigma-Aldrich) and 50 μg/mL gentamycin. Where applicable, Vitamin C (L-ascorbic acid), Coenzyme Q10 (ubiquinone) or mitoTEMPO (all from Sigma Aldrich) were added to the differentiation medium at final concentrations of 20 μM for each antioxidant compound.

Cell culture under hypoxic conditions was performed in a commercially available humidified hypoxia chamber (STEMCELL technologies, Cambridge, UK) in an incubator at 37 °C. To keep O_2 tension constant, the hypoxia chamber was injected with a gas mixture of 1% O_2, 5% CO_2 and 94% N_2 (Air Liquide, London, UK) at continuous flow rate of approximately 1 L/min. For medium changes in hypoxic cultures, e.g. for RONS and hypoxia measurements or antioxidant treatment, all medium, buffer and reagent solutions were preconditioned in 1% O_2, 5% CO_2 and 94% N_2 for at least the experimental duration, or, for longer experiments in differentiation, for at least 24 h.

4.3. ROS measurements

For ROS measurements in proliferating myoblasts, 10,000 cells/well were seeded into black, clear-bottom polystyrene 96-well plates (Corning®, Sigma Aldrich) and assayed 24 h later. For measurements in hypoxia, 5000 cells/well were seeded, transferred into hypoxia the following day and assayed 24 h later, with reagents preconditioned in 1% O_2, 5% CO_2 and 94% N_2 for 24 h. To assess ROS levels in differentiated myotubes, 50,000 cells/well were seeded into black, clear-bottom polystyrene 96-well plates, and switched to differentiation 24 h later. ROS measurements were performed in myotubes after 3 days of differentiation (in normoxia or hypoxia). ROS probes used and staining conditions are detailed in Table 1.

ROS measurements were performed in Hank's Balanced Salt Solution (HBSS) supplemented with Ca^{2+} and Mg^{2+} (Sigma Aldrich). Cells were washed twice with HBSS, followed by incubation with the respective fluorescent ROS probe and HOECHST33342 (0.5 μg/mL; ThermoFisher Scientific) in HBSS for 30 min in the dark. After staining, cells were washed twice with HBSS and fluorescence intensity was measured on a POLARStar Omega microplate reader (BMG Labtech, Aylesbury, UK) in orbital averaging scan mode (20 flashes per well, scan diameter 4 mm). For normalisation to cell number, ROS probe fluorescence was normalized to DNA content as simultaneously assessed via HOECHST 33342 fluorescence in the same well.

4.4. Assessment of $\Delta\Psi m$ and mitochondrial lipid peroxidation

ΔΨm was assessed by Tetramethylrhodamine methyl ester (TMRM; Sigma Aldrich) staining in black clear-bottom polystyrene 96-well plates. Briefly, cells were washed twice with HBSS and subsequently stained with 100 nM TMRM and 0.5 μg/mL HOECHST33342 in HBSS for 30 min at 37 °C in the dark. After staining, cells were washed twice with HBSS and fluorescence intensity was measured on a POLARStar Omega microplate reader in orbital averaging scan mode (20 flashes per well, scan diameter 4 mm). For normalisation to cell number, TMRM fluorescence was normalized to DNA content as simultaneously assessed via HOECHST 33342 in the same well.

Mitochondrial lipid peroxidation was measured with the ratiomeric C11-BODIPY derivative MitoPerOx (Abcam, Cambridge, UK). For iDUX4 myoblasts in proliferation, 25,000 cells/well were seeded into black clear-bottom polystyrene 96-well plates and, after 24 h, induced to

Table 1
Fluorescent probes used for RONS measurements.

Species	Probe	Supplier	Conc.	Staining duration	λ Ex/Em
General (cytoplasmic) ROS	CM-H_2DCFDA	ThermoFisher Scientific	5 uM	30 min (in HBSS)	485/520
mitoROS	MitoTracker® Red CM-H_2XROS	ThermoFisher Scientific	250 nM	30 min (in HBSS)	584/620

express DUX4 for 16 h. For measurements in iDUX4 myotubes, 50,000 cells/well were seeded and differentiation induced 24 h later. After 36 h, when myotube formation was evident, DUX4 expression was induced for 24 h with subsequent assaying. For staining, cells were washed twice with HBSS and incubated with 100 nM MitoPerOx probe in HBSS for 45 min at 37 °C in the dark. After staining, cells were washed twice with HBSS and fluorescence intensity was measured on a POLARStar Omega microplate reader in orbital averaging scan mode (20 flashes per well, scan diameter 4 mm). Mitochondrial lipid peroxidation was quantified by calculating the ratio between MitoPerOx fluorescence intensity at em520/em590 after excitation at 488 nm.

4.5. Metabolic activity measurement

Metabolic activity was measured using the luminescence RealTime-Glo™ MT Cell Viability assay (Promega, Southampton, UK) with a modified protocol. In proliferation, 5000 iDUX4 cells/well were seeded into opaque walled polystyrene 96-well plates (Corning®, Sigma Aldrich). 24 h later, DUX4 expression was induced and assay substrates were added simultaneously for longitudinal assaying for up to 16 h according to the manufacturer's protocol. Luminescence was read with a Mithras LB940 multimode microplate reader (Berthold Technologies, Bad Wildbad, Germany) at 0.1s exposure, and metabolic activity was calculated as the ratio between luminescent signal and DNA content, as assessed through HOECHST33342 fluorescence from sister cultures undergoing the same treatment.

For iDUX4 myotubes, the assay was used in an end-point format. Briefly, 50,000 cells/well were seeded into opaque 96-well plates and induced to differentiate 24 h later. After 36 h, DUX4 expression was induced for 24 h (with simultaneous antioxidant supplementation where applicable) and, at the end of the experimental treatment duration, assay substrates were added according to the manufacturer's protocol. Luminescence was read after 3 h incubation with the MT assay substrates, and metabolic activity calculated as described above.

4.6. Apoptosis and necrosis assaying

Apoptosis and Necrosis were assayed with the combined luminescence/fluorescence RealTime-Glo™ Annexin V Apoptosis and Necrosis assay (Promega), according to the manufacturer's instructions. 5000 iDUX4 cells/well were seeded into black clear-bottom polystyrene 96-well plates. 24 h later, cells were induced to express DUX4 and assay substrates were added simultaneously for longitudinal assaying of apoptosis/necrosis for up to 24 h. Apoptosis was quantified as luminescent signal intensity, as assessed on a Mithras LB940 multimode microplate reader (0.1s exposure), and necrosis was quantified as fluorescence intensity (ex488/em520), as assessed on a POLARStar Omega microplate reader in orbital averaging scan mode (20 flashes per well, scan diameter 4 mm).

4.7. High resolution respirometry (HRR)

Respirometric analysis was performed on an Oroboros O2k oxygraph (Oroboros Instruments, Innsbruck, Austria). In proliferation, 4×10^6 viable iDUX4 myoblasts were used per experiment (after 16 h of DUX4 expression). Cell viability was assessed by trypan Blue (Sigma Aldrich) staining prior to each respirometric analysis, and oxygen consumption rate normalized to cell number. For respirometric analysis of iDUX4 myotubes, 5.86×10^6 cells were seeded per 75 cm^2 cell culture flasks (Nunc™, ThermoFisher Scientific), and switched to differentiation 24 h later. After 36 h, after myotubes had formed, DUX4 expression was induced for another 24 h, and measurements performed from myotubes harvested by trypsination. To account for differential cell/myotube amounts, DNA quantitation of sister cultures undergoing the same treatment was performed by HOECHST33342 staining, as described above, and HEOCHST33342 fluorescence subsequently used as normaliser for oxygen consumption rate.

Respiratory states were analysed through substrate-uncoupler-inhibitor-titration (SUIT) as follows: to assess Complex I- and Complex II-linked respiration, cells were incubated in a buffer containing 80 mM KCl, 5 mM KH_2PO_4, 50 mM 3-(N-morpholino)propanesulfonic acid, 1 mM ethylene glycol-bis(2-aminoethylether)-N,N,N′,N'-tetraacetic acid, and 1 mg/mL fatty acid-free bovine serum albumin (pH 7.4, 37 °C) [127], and permeabilized with digitonin (8 μM). State 4 respiration (LEAK) was induced either by the addition of 5 mM glutamate and 5 mM malate (complex I), 10 mM pyruvate (complex I), or 10 mM succinate in the presence of 1.4 μM rotenone (complex II). State 3 respiration (OXPHOS) was stimulated by the addition of 1 mM adenosine diphosphate. Maximum electron transfer system capacity (max. ETS) was measured by titration of carbonyl cyanide-4-(trifluoromethoxy) phenylhydrazone in steps of 0.1 μM. To calculate respiratory control ratio (RCR), State 3 respiration (OXPHOS) was divided by State 4 respiration (LEAK). Oxygen consumption rates were obtained by calculating the negative time derivative of the measured oxygen concentration.

4.8. Cellular hypoxia measurement

Cellular oxygenation was determined with the fluorescent O_2-sensitive hypoxia indicator Image-IT™ Green Hypoxia Reagent (ThermoFisher Scientific) according to the manufacturer's instructions. Cells seeded in black clear-bottom polystyrene 96-well plates were incubated with 5 μM Green Hypoxia Reagent in growth or differentiation medium, respectively, for 30 min at 37 °C in the dark. Subsequently, cells were washed with HBSS, treated with DOX (for DUX4 expression in iDUX4 cells) and/or antioxidants and transferred to 1% O_2, 5% CO_2 and 94% N_2 for the appropriate remaining culture period (e.g. 16 h for iDUX4 myoblasts induced to express DUX4 or 24 h for antioxidant treatment in iDUX4 or FSHD myotubes). To quantify cellular hypoxia, cells were washed twice with HBSS and hypoxia indicator fluorescence intensity (ex488/em520) measured on a POLARStar Omega microplate reader in orbital averaging scan mode (20 flashes per well, scan diameter 4 mm). Afterwards, DNA content was determined for normalisation by staining with 0.5 μg/mL HOECHST33342 in HBSS for 30 min at 37 °C in the dark, and subsequently reading HOECHST33342 fluorescence intensity. For visualization of Green Hypoxia Reagent fluorescence, fluorescence micrographs were taken on a Zeiss Axiovert 200 M epifluorescence microscope using a Zeiss AxioCam HRm and AxioVision 4.4 software (Zeiss, Jena, Germany).

4.9. Immunofluorescence microscopy

For immunolabelling, cells were fixed with 4% paraformaldehyde/PBS (Alfa Aesar, Heysham, UK) for 10 min, washed three times with PBS for 5 min each, then permeabilised with 0.1% Triton-X/PBS (Sigma Aldrich) for 15 min and washed three times with PBS. Blocking was performed in 5% normal goat serum (GS)/PBS (Dako, Glostrup, Denmark) for 60 min, and, after three washes with PBS, cells were incubated with primary antibody in 1% GS/PBS on a rocker overnight at 4 °C. Cells were then washed three times with PBS, and incubated with secondary antibody in 1% GS/PBS for 60 min in the dark at room temperature. After three washes with PBS, nuclei were stained with 0.5 μg/mL HOECHST33342 in PBS for 10 min, washed again with PBS and imaged on a Zeiss Axiovert 200 M epifluorescence microscope using a Zeiss AxioCam HRm and AxioVision 4.4 software.

Primary antibodies were mouse anti-MyHC (1:400; MF-20; Developmental Studies Hybridoma Bank, IA, USA), mouse anti-DUX4 (1:500; clone 9A12; Merck Millipore, Croxley Park, UK) and rabbit anti-HIF1α (1:500; EP1215Y, Abcam). Secondary antibodies were goat anti-mouse IgG (H + L) AlexaFluor-488 (1:500, A-11001, ThermoFisher Scientific) and goat anti-rabbit IgG (H + L) AlexaFluor-594 (1:500, A-11012, ThermoFisher Scientific).

4.10. Determination of MyHC-positive area and differentiation index

Image analysis was performed from MyHC immunofluorescence micrographs with a custom-made high-throughput image analysis software, as recently described (software provided as suppl. file 1 in Ref. [52]). For determination of the MyHC-positive area, at least three fluorescence micrographs were taken per well. Briefly, the software first splits each image into separate channels (e.g. the MyHC and nuclear counterstain channels). The channel displaying MyHC is then passed through a low pass filter and a size filter is applied to remove background labelling in the binarized image. The positive proportion of the image is then quantified as MyHC-positive area. The mean MyHC-positive area per well was calculated as the average from three representative images per well. Likewise, differentiation index was automatically determined from the same images as the percentage of nuclei within the MyHC-positive area.

4.11. Statistical analysis

Statistical analysis was performed using GraphPad Prism version 9.1.2 for Windows (GraphPad Software, San Diego, CA, USA; www.graphpad.com). Experiments were performed at least 3 independent times, with detailed N numbers and technical replicates given in each figure. Variance between groups was compared using a Brown Forsythe test and revealed no significant difference. A comparison between two groups was performed using an unpaired homoscedastic two-tailed student's *t*-test. A comparison of more than two groups was performed using a one-way analysis of variance (ANOVA) followed by either Dunnett's post-test when different groups were compared with the control group or Tukey's post-test when different groups were compared with each other. $p < 0.05$ was considered significantly different, with p values indicated for each significant comparison in the figures.

Funding

PH was mainly funded by the Medical Research Council (MR/P023215/1) and then by an Erwin Schroedinger post-doctoral fellowship awarded by the Austrian Science Fund (FWF, J4435-B), supported by Friends of FSH Research (Project 936,270) and the FSHD Society (FSHD-Fall2020-3308289076). MG was supported by the Medical Research Council (MR/S002472/1), EE was funded by Wellcome Trust PhD Studentship (WT 222352/Z/21/Z), as was JP (WT 203949/Z/16/Z) initially and then Muscular Dystrophy UK (19GRO-PG12-0493). THN was supported by the FRIA grant of the Fonds de la Recherche Scientifique (FRS-FNRS) and by the Association Les Amis F.S.H. (Amis FSH).

Author contributions

PSZ with CRSB obtained funding for the project. PH, AT, A-ED, CRSB, JG, AVK and PSZ designed the research study and wrote the draft manuscript. PH, MG, AW, ENE, JP and THN conducted experiments and acquired and analysed data. KM provided cell lines. PSZ and PH finalised manuscript, collated data and secured additional support funding.

Declaration of competing interest

The authors declare that they have no conflicts of interest.

Acknowledgements

We would like to thank: Vincent Mouly (Center for Research In Myology, UMRS 974 Sorbonne Université-INSERM, Paris, France) and Charles P. Emerson (Wellstone Muscular Dystrophy Program, University of Massachusetts Medical School, MA, USA) for providing immortalised myoblast lines; Sara Badodi for vital assistance in RNAseq analysis and data visualisation; Alexandra Belayew, Luca Pinton, Terje Wimberger, Christian Oeffel, Dominik Hanetseder and Matthias Gloeckel for helpful discussion; Johannes Oesterreicher, Nadja Milivojev and Sergejs Zavadskis for useful input on ROS measurements.

Appendix B. Supplementary information

Supplementary data to this article can be found online at https://doi.org/10.1016/j.redox.2022.102251.

References

[1] J.C. Deenen, et al., Population-based incidence and prevalence of facioscapulohumeral dystrophy, Neurology 83 (12) (2014) 1056–1059.
[2] R. Sposito, et al., Facioscapulohumeral muscular dystrophy type 1A in northwestern Tuscany: a molecular genetics-based epidemiological and genotype-phenotype study, Genet. Test. 9 (1) (2005) 30–36.
[3] R. Tawil, S.M. Van Der Maarel, Facioscapulohumeral muscular dystrophy, Muscle Nerve 34 (1) (2006) 1–15.
[4] C.R.S. Banerji, P.S. Zammit, Pathomechanisms and biomarkers in facioscapulohumeral muscular dystrophy: roles of DUX4 and PAX7, EMBO Mol. Med. 13 (2021), e13695.
[5] S. Pandya, W.M. King, R. Tawil, Facioscapulohumeral dystrophy, Phys. Ther. 88 (1) (2008) 105–113.
[6] K.L. Lutz, et al., Clinical and genetic features of hearing loss in facioscapulohumeral muscular dystrophy, Neurology 81 (16) (2013) 1374–1377.
[7] R.B. Fitzsimons, Retinal vascular disease and the pathogenesis of facioscapulohumeral muscular dystrophy. A signalling message from Wnt? Neuromuscul. Disord. 21 (4) (2011) 263–271.
[8] P. Sakellariou, et al., Mutation spectrum and phenotypic manifestation in FSHD Greek patients, Neuromuscul. Disord. 22 (4) (2012) 339–349.
[9] R. Tawil, et al., Extreme variability of expression in monozygotic twins with FSH muscular dystrophy, Neurology 43 (2) (1993) 345–348.
[10] M.M. Tonini, et al., Asymptomatic carriers and gender differences in facioscapulohumeral muscular dystrophy (FSHD), Neuromuscul. Disord. 14 (1) (2004) 33–38.
[11] P. Calandra, et al., Allele-specific DNA hypomethylation characterises FSHD1 and FSHD2, J. Med. Genet. 53 (5) (2016) 348–355.
[12] J. Gabriels, et al., Nucleotide sequence of the partially deleted D4Z4 locus in a patient with FSHD identifies a putative gene within each 3.3 kb element, Gene 236 (1) (1999) 25–32.
[13] J.E. Hewitt, et al., Analysis of the tandem repeat locus D4Z4 associated with facioscapulohumeral muscular dystrophy, Hum. Mol. Genet. 3 (8) (1994) 1287–1295.
[14] J.C. van Deutekom, et al., FSHD associated DNA rearrangements are due to deletions of integral copies of a 3.2 kb tandemly repeated unit, Hum. Mol. Genet. 2 (12) (1993) 2037–2042.
[15] P.G. van Overveld, et al., Hypomethylation of D4Z4 in 4q-linked and non-4q-linked facioscapulohumeral muscular dystrophy, Nat. Genet. 35 (4) (2003) 315–317.
[16] C. Wijmenga, et al., Chromosome 4q DNA rearrangements associated with facioscapulohumeral muscular dystrophy, Nat. Genet. 2 (1) (1992) 26–30.
[17] V. Kowaljow, et al., The DUX4 gene at the FSHD1A locus encodes a pro-apoptotic protein, Neuromuscul. Disord. 17 (8) (2007) 611–623.
[18] R.J. Lemmers, et al., A unifying genetic model for facioscapulohumeral muscular dystrophy, Science 329 (5999) (2010) 1650–1653.
[19] R. Tupler, et al., Monosomy of distal 4q does not cause facioscapulohumeral muscular dystrophy, J. Med. Genet. 33 (5) (1996) 366–370.
[20] R.J. Lemmers, et al., Digenic inheritance of an SMCHD1 mutation and an FSHD-permissive D4Z4 allele causes facioscapulohumeral muscular dystrophy type 2, Nat. Genet. 44 (12) (2012) 1370–1374.
[21] M.L. van den Boogaard, et al., Mutations in DNMT3B modify epigenetic repression of the D4Z4 repeat and the penetrance of facioscapulohumeral dystrophy, Am. J. Hum. Genet. 98 (5) (2016) 1020–1029.
[22] K. Hamanaka, et al., Homozygous nonsense variant in LRIF1 associated with facioscapulohumeral muscular dystrophy, Neurology 94 (23) (2020) e2441–e2447.
[23] N. Jansz, et al., The epigenetic regulator SMCHD1 in development and disease, Trends Genet. 33 (4) (2017) 233–243.
[24] R. Tawil, et al., Evidence-based guideline summary: evaluation, diagnosis, and management of facioscapulohumeral muscular dystrophy: report of the guideline development, dissemination, and implementation subcommittee of the American academy of neurology and the practice issues review panel of the American association of neuromuscular & electrodiagnostic medicine, Neurology 85 (4) (2015) 357–364.
[25] I. Scionti, et al., Large-scale population analysis challenges the current criteria for the molecular diagnosis of fascioscapulohumeral muscular dystrophy, Am. J. Hum. Genet. 90 (4) (2012) 628–635.
[26] G. Ricci, et al., Large genotype-phenotype study in carriers of D4Z4 borderline alleles provides guidance for facioscapulohumeral muscular dystrophy diagnosis, Sci. Rep. 10 (1) (2020) 21648.
[27] L. Ruggiero, et al., Phenotypic variability among patients with D4Z4 reduced allele facioscapulohumeral muscular dystrophy, JAMA Netw. Open 3 (5) (2020) e204040.

[28] L.M. Wallace, et al., DUX4, a candidate gene for facioscapulohumeral muscular dystrophy, causes p53-dependent myopathy in vivo, Ann. Neurol. 69 (3) (2011) 540–552.
[29] H. Xu, et al., Dux4 induces cell cycle arrest at G1 phase through upregulation of p21 expression, Biochem. Biophys. Res. Commun. 446 (1) (2014) 235–240.
[30] P. Knopp, et al., DUX4 induces a transcriptome more characteristic of a less-differentiated cell state and inhibits myogenesis, J. Cell Sci. 129 (20) (2016) 3816–3831.
[31] D. Bosnakovski, et al., DUX4c, an FSHD candidate gene, interferes with myogenic regulators and abolishes myoblast differentiation, Exp. Neurol. 214 (1) (2008) 87–96.
[32] D. Bosnakovski, et al., An isogenetic myoblast expression screen identifies DUX4-mediated FSHD-associated molecular pathologies, EMBO J. 27 (20) (2008) 2766–2779.
[33] C.R.S. Banerji, et al., PAX7 target genes are globally repressed in facioscapulohumeral muscular dystrophy skeletal muscle, Nat. Commun. 8 (1) (2017) 2152.
[34] C.R.S. Banerji, P.S. Zammit, PAX7 target gene repression is a superior FSHD biomarker than DUX4 target gene activation, associating with pathological severity and identifying FSHD at the single-cell level, Hum. Mol. Genet. 28 (13) (2019) 2224–2236.
[35] T.A. Rando, Role of nitric oxide in the pathogenesis of muscular dystrophies: a "two hit" hypothesis of the cause of muscle necrosis, Microsc. Res. Tech. 55 (4) (2001) 223–235.
[36] J.G. Tidball, M. Wehling-Henricks, The role of free radicals in the pathophysiology of muscular dystrophy, J. Appl. Physiol. 102 (4) (2007) 1677–1686.
[37] A. Toscano, et al., Oxidative stress in myotonic dystrophy type 1, Free Radic. Res. 39 (7) (2005) 771–776.
[38] I. Kramerova, et al., Mitochondrial abnormalities, energy deficit and oxidative stress are features of calpain 3 deficiency in skeletal muscle, Hum. Mol. Genet. 18 (17) (2009) 3194–3205.
[39] J.R. Terrill, et al., Oxidative stress and pathology in muscular dystrophies: focus on protein thiol oxidation and dysferlinopathies, FEBS J. 280 (17) (2013) 4149–4164.
[40] S.T. Winokur, et al., Facioscapulohumeral muscular dystrophy (FSHD) myoblasts demonstrate increased susceptibility to oxidative stress, Neuromuscul. Disord. 13 (4) (2003) 322–333.
[41] B. Celegato, et al., Parallel protein and transcript profiles of FSHD patient muscles correlate to the D4Z4 arrangement and reveal a common impairment of slow to fast fibre differentiation and a general deregulation of MyoD-dependent genes, Proteomics 6 (19) (2006) 5303–5321.
[42] S. Cheli, et al., Expression profiling of FSHD-1 and FSHD-2 cells during myogenic differentiation evidences common and distinctive gene dysregulation patterns, PLoS One 6 (6) (2011) e20966.
[43] D. Laoudj-Chenivesse, et al., Increased levels of adenine nucleotide translocator 1 protein and response to oxidative stress are early events in facioscapulohumeral muscular dystrophy muscle, J. Mol. Med. (Berl.) 83 (3) (2005) 216–224.
[44] V. Macaione, et al., RAGE-NF-kappaB pathway activation in response to oxidative stress in facioscapulohumeral muscular dystrophy, Acta Neurol. Scand. 115 (2) (2007) 115–121.
[45] V. Sharma, et al., DUX4 differentially regulates transcriptomes of human rhabdomyosarcoma and mouse C2C12 cells, PLoS One 8 (5) (2013) e64691.
[46] A. Turki, et al., Functional muscle impairment in facioscapulohumeral muscular dystrophy is correlated with oxidative stress and mitochondrial dysfunction, Free Radic. Biol. Med. 53 (5) (2012) 1068–1079.
[47] Y. Bou Saada, et al., Facioscapulohumeral dystrophy myoblasts efficiently repair moderate levels of oxidative DNA damage, Histochem. Cell Biol. 145 (4) (2016) 475–483.
[48] P. Dmitriev, et al., DUX4-induced constitutive DNA damage and oxidative stress contribute to aberrant differentiation of myoblasts from FSHD patients, Free Radic. Biol. Med. 99 (2016) 244–258.
[49] M.P. Murphy, How mitochondria produce reactive oxygen species, Biochem. J. 417 (1) (2009) 1–13.
[50] L.W. Thomas, M. Ashcroft, Exploring the molecular interface between hypoxia-inducible factor signalling and mitochondria, Cell. Mol. Life Sci. 76 (9) (2019) 1759–1777.
[51] E. Le Moal, et al., Redox control of skeletal muscle regeneration, Antioxidants Redox Signal. 27 (5) (2017) 276–310.
[52] C.R.S. Banerji, et al., Dynamic transcriptomic analysis reveals suppression of PGC1alpha/ERRalpha drives perturbed myogenesis in facioscapulohumeral muscular dystrophy, Hum. Mol. Genet. 28 (8) (2019) 1244–1259.
[53] M. Barro, et al., Myoblasts from affected and non-affected FSHD muscles exhibit morphological differentiation defects, J. Cell Mol. Med. 14 (1–2) (2010) 275–289.
[54] C.R. Banerji, et al., beta-Catenin is central to DUX4-driven network rewiring in facioscapulohumeral muscular dystrophy, J. R. Soc. Interface 12 (102) (2015) 20140797.
[55] A. Lek, et al., Applying genome-wide CRISPR-Cas9 screens for therapeutic discovery in facioscapulohumeral muscular dystrophy, Sci. Transl. Med. 12 (536) (2020).
[56] A.P. Denny, A.K. Heather, Are antioxidants a potential therapy for FSHD? A review of the literature, Oxid. Med. Cell. Longev. 2017 (2017) 7020295.
[57] D. Bosnakovski, et al., High-throughput screening identifies inhibitors of DUX4-induced myoblast toxicity, Skeletal Muscle 4 (1) (2014) 4.
[58] M. Sasaki-Honda, et al., A patient-derived iPSC model revealed oxidative stress increases facioscapulohumeral muscular dystrophy-causative DUX4, Hum. Mol. Genet. 27 (23) (2018) 4024–4035.
[59] P. Emilie, et al., Oxidative stress and dystrophy Facioscapulohumeral: effects of vitamin C, vitamin E, zinc gluconate and selenomethionine supplementation, Free Radic. Biol. Med. 75 (Suppl 1) (2014) S14.
[60] E. Passerieux, et al., Effects of vitamin C, vitamin E, zinc gluconate, and selenomethionine supplementation on muscle function and oxidative stress biomarkers in patients with facioscapulohumeral dystrophy: a double-blind randomized controlled clinical trial, Free Radic. Biol. Med. 81 (2015) 158–169.
[61] A. Karpukhina, et al., Analysis of genes regulated by DUX4 via oxidative stress reveals potential therapeutic targets for treatment of facioscapulohumeral dystrophy, Redox Biol. 43 (2021) 102008.
[62] L.H. Wang, et al., MRI-informed muscle biopsies correlate MRI with pathology and DUX4 target gene expression in FSHD, Hum. Mol. Genet. 28 (3) (2019) 476–486.
[63] J.W. Taanman, The mitochondrial genome: structure, transcription, translation and replication, Biochim. Biophys. Acta 1410 (2) (1999) 103–123.
[64] L.D. Zorova, et al., Mitochondrial membrane potential, Anal. Biochem. 552 (2018) 50–59.
[65] S.S. Korshunov, V.P. Skulachev, A.A. Starkov, High protonic potential actuates a mechanism of production of reactive oxygen species in mitochondria, FEBS Lett. 416 (1) (1997) 15–18.
[66] S. Jagannathan, et al., Model systems of DUX4 expression recapitulate the transcriptional profile of FSHD cells, Hum. Mol. Genet. 25 (20) (2016) 4419–4431.
[67] D. Bhattacharya, A. Scime, Mitochondrial function in muscle stem cell fates, Front. Cell Dev. Biol. 8 (2020) 480.
[68] S. Haramizu, et al., Dietary resveratrol confers apoptotic resistance to oxidative stress in myoblasts, J. Nutr. Biochem. 50 (2017) 103–115.
[69] G. Olah, et al., Differentiation-associated downregulation of poly(ADP-ribose) polymerase-1 expression in myoblasts serves to increase their resistance to oxidative stress, PLoS One 10 (7) (2015) e0134227.
[70] T. Hagen, et al., Redistribution of intracellular oxygen in hypoxia by nitric oxide: effect on HIF1alpha, Science 302 (5652) (2003) 1975–1978.
[71] R.B. Hamanaka, N.S. Chandel, Mitochondrial reactive oxygen species regulate hypoxic signaling, Curr. Opin. Cell Biol. 21 (6) (2009) 894–899.
[72] G. Solaini, et al., Hypoxia and mitochondrial oxidative metabolism, Biochim. Biophys. Acta 1797 (6–7) (2010) 1171–1177.
[73] F. Pala, et al., Distinct metabolic states govern skeletal muscle stem cell fates during prenatal and postnatal myogenesis, J. Cell Sci. 131 (14) (2018) jcs212977.
[74] J. Sin, et al., Mitophagy is required for mitochondrial biogenesis and myogenic differentiation of C2C12 myoblasts, Autophagy 12 (2) (2016) 369–380.
[75] J. Magalhaes, et al., Acute and severe hypobaric hypoxia increases oxidative stress and impairs mitochondrial function in mouse skeletal muscle, J. Appl. Physiol. 99 (4) (2005) 1247–1253.
[76] A.J. Bittel, et al., Membrane repair deficit in facioscapulohumeral muscular dystrophy, Int. J. Mol. Sci. 21 (15) (2020) 5575.
[77] A. Tassin, et al., DUX4 expression in FSHD muscle cells: how could such a rare protein cause a myopathy? J. Cell Mol. Med. 17 (1) (2013) 76–89.
[78] J.M. Suski, et al., Relation between mitochondrial membrane potential and ROS formation, Methods Mol. Biol. 810 (2012) 183–205.
[79] B. Lipinski, Hydroxyl radical and its scavengers in health and disease, Oxid. Med. Cell. Longev. 2011 (2011) 809696.
[80] R. Radi, Oxygen radicals, nitric oxide, and peroxynitrite: redox pathways in molecular medicine, Proc. Natl. Acad. Sci. U. S. A. 115 (23) (2018) 5839–5848.
[81] G.C. Brown, Nitric oxide and mitochondrial respiration, Biochim. Biophys. Acta 1411 (2–3) (1999) 351–369.
[82] G.C. Brown, V. Borutaite, Inhibition of mitochondrial respiratory complex I by nitric oxide, peroxynitrite and S-nitrosothiols, Biochim. Biophys. Acta 1658 (1–2) (2004) 44–49.
[83] J.D. Erusalimsky, S. Moncada, Nitric oxide and mitochondrial signaling: from physiology to pathophysiology, Arterioscler. Thromb. Vasc. Biol. 27 (12) (2007) 2524–2531.
[84] A. Galkin, A. Higgs, S. Moncada, Nitric oxide and hypoxia, Essays Biochem. 43 (2007) 29–42.
[85] C.T. Taylor, S. Moncada, Nitric oxide, cytochrome C oxidase, and the cellular response to hypoxia, Arterioscler. Thromb. Vasc. Biol. 30 (4) (2010) 643–647.
[86] B. Brune, Nitric oxide: NO apoptosis or turning it ON? Cell Death Differ. 10 (8) (2003) 864–869.
[87] P.K. Kim, et al., The regulatory role of nitric oxide in apoptosis, Int. Immunopharm. 1 (8) (2001) 1421–1441.
[88] L. Kussmaul, J. Hirst, The mechanism of superoxide production by NADH: ubiquinone oxidoreductase (complex I) from bovine heart mitochondria, Proc. Natl. Acad. Sci. U. S. A. 103 (20) (2006) 7607–7612.
[89] M.D. Brand, The sites and topology of mitochondrial superoxide production, Exp. Gerontol. 45 (7–8) (2010) 466–472.
[90] M. Forkink, et al., Mitochondrial hyperpolarization during chronic complex I inhibition is sustained by low activity of complex II, III, IV and V, Biochim. Biophys. Acta 1837 (8) (2014) 1247–1256.
[91] C. Giovannini, et al., Mitochondria hyperpolarization is an early event in oxidized low-density lipoprotein-induced apoptosis in Caco-2 intestinal cells, FEBS Lett. 523 (1–3) (2002) 200–206.
[92] M. Piacentini, et al., Transglutaminase overexpression sensitizes neuronal cell lines to apoptosis by increasing mitochondrial membrane potential and cellular oxidative stress, J. Neurochem. 81 (5) (2002) 1061–1072.

[93] M.Y. Vyssokikh, et al., Mild depolarization of the inner mitochondrial membrane is a crucial component of an anti-aging program, Proc. Natl. Acad. Sci. U. S. A. 117 (12) (2020) 6491–6501.
[94] A.J. Lambert, M.D. Brand, Superoxide production by NADH:ubiquinone oxidoreductase (complex I) depends on the pH gradient across the mitochondrial inner membrane, Biochem. J. 382 (Pt 2) (2004) 511–517.
[95] C. Chinopoulos, V. Adam-Vizi, Mitochondria as ATP consumers in cellular pathology, Biochim. Biophys. Acta 1802 (1) (2010) 221–227.
[96] W. Xu, I.G. Charles, S. Moncada, Nitric oxide: orchestrating hypoxia regulation through mitochondrial respiration and the endoplasmic reticulum stress response, Cell Res. 15 (1) (2005) 63–65.
[97] E. Barbieri, P. Sestili, Reactive oxygen species in skeletal muscle signaling, J Signal Transduct 2012 (2012) 982794.
[98] D. Malinska, et al., Changes in mitochondrial reactive oxygen species synthesis during differentiation of skeletal muscle cells, Mitochondrion 12 (1) (2012) 144–148.
[99] C.D. Moyes, et al., Mitochondrial biogenesis during cellular differentiation, Am. J. Physiol. 272 (4 Pt 1) (1997) C1345–C1351.
[100] A.H. Remels, et al., Regulation of mitochondrial biogenesis during myogenesis, Mol. Cell. Endocrinol. 315 (1–2) (2010) 113–120.
[101] A. Wagatsuma, K. Sakuma, Mitochondria as a potential regulator of myogenesis, Sci. World J. 2013 (2013) 593267.
[102] T.L. Clanton, Hypoxia-induced reactive oxygen species formation in skeletal muscle, J. Appl. Physiol. 102 (6) (2007) 2379–2388.
[103] G.B. Waypa, et al., Increases in mitochondrial reactive oxygen species trigger hypoxia-induced calcium responses in pulmonary artery smooth muscle cells, Circ. Res. 99 (9) (2006) 970–978.
[104] N.S. Chandel, et al., Mitochondrial reactive oxygen species trigger hypoxia-induced transcription, Proc. Natl. Acad. Sci. U. S. A. 95 (20) (1998) 11715–11720.
[105] N.S. Chandel, et al., Reactive oxygen species generated at mitochondrial complex III stabilize hypoxia-inducible factor-1alpha during hypoxia: a mechanism of O2 sensing, J. Biol. Chem. 275 (33) (2000) 25130–25138.
[106] E.L. van der Kooi, et al., No effect of folic acid and methionine supplementation on D4Z4 methylation in patients with facioscapulohumeral muscular dystrophy, Neuromuscul. Disord. 16 (11) (2006) 766–769.
[107] M.P. Murphy, Antioxidants as therapies: can we improve on nature? Free Radic. Biol. Med. 66 (2014) 20–23.
[108] B.J. Snow, et al., A double-blind, placebo-controlled study to assess the mitochondria-targeted antioxidant MitoQ as a disease-modifying therapy in Parkinson's disease, Mov. Disord. 25 (11) (2010) 1670–1674.
[109] E.J. Gane, et al., The mitochondria-targeted anti-oxidant mitoquinone decreases liver damage in a phase II study of hepatitis C patients, Liver Int. 30 (7) (2010) 1019–1026.
[110] A. Petrov, et al., SkQ1 ophthalmic solution for dry eye treatment: results of a phase 2 safety and efficacy clinical study in the environment and during challenge in the controlled adverse environment model, Adv. Ther. 33 (1) (2016) 96–115.
[111] B.D. E, G. Marfany, The relevance of oxidative stress in the pathogenesis and therapy of retinal dystrophies, Antioxidants 9 (4) (2020) 347.
[112] F. Forli, et al., Mitochondrial syndromic sensorineural hearing loss, Biosci. Rep. 27 (1–3) (2007) 113–123.
[113] H. Kokotas, M.B. Petersen, P.J. Willems, Mitochondrial deafness, Clin. Genet. 71 (5) (2007) 379–391.
[114] E. Tavanai, G. Mohammadkhani, Role of antioxidants in prevention of age-related hearing loss: a review of literature, Eur. Arch. Oto-Rhino-Laryngol. 274 (4) (2017) 1821–1834.
[115] C. Fujimoto, T. Yamasoba, Mitochondria-targeted antioxidants for treatment of hearing loss: a systematic review, Antioxidants 8 (4) (2019) 109.
[116] Q. Jiang, et al., Mitochondria-targeted antioxidants: a step towards disease treatment, Oxid. Med. Cell. Longev. 2020 (2020) 8837893.
[117] A.O. Oyewole, M.A. Birch-Machin, Mitochondria-targeted antioxidants, Faseb. J. 29 (12) (2015) 4766–4771.
[118] S. Jagannathan, et al., Quantitative proteomics reveals key roles for post-transcriptional gene regulation in the molecular pathology of facioscapulohumeral muscular dystrophy, Elife 8 (2019) e41740.
[119] S. Badodi, et al., Inositol treatment inhibits medulloblastoma through suppression of epigenetic-driven metabolic adaptation, Nat. Commun. 12 (1) (2021) 2148.
[120] S. Tarazona, et al., Data quality aware analysis of differential expression in RNA-seq with NOISeq R/Bioc package, Nucleic Acids Res. 43 (21) (2015) e140.
[121] S. Durinck, et al., Mapping identifiers for the integration of genomic datasets with the R/Bioconductor package biomaRt, Nat. Protoc. 4 (8) (2009) 1184–1191.
[122] M.D. Robinson, D.J. McCarthy, G.K. Smyth, edgeR: a Bioconductor package for differential expression analysis of digital gene expression data, Bioinformatics 26 (1) (2010) 139–140.
[123] P. Shannon, et al., Cytoscape: a software environment for integrated models of biomolecular interaction networks, Genome Res. 13 (11) (2003) 2498–2504.
[124] Y.D. Krom, et al., Generation of isogenic D4Z4 contracted and noncontracted immortal muscle cell clones from a mosaic patient: a cellular model for FSHD, Am. J. Pathol. 181 (4) (2012) 1387–1401.
[125] S. Homma, et al., A unique library of myogenic cells from facioscapulohumeral muscular dystrophy subjects and unaffected relatives: family, disease and cell function, Eur. J. Hum. Genet. 20 (4) (2012) 404–410.
[126] S.H. Choi, et al., DUX4 recruits p300/CBP through its C-terminus and induces global H3K27 acetylation changes, Nucleic Acids Res. 44 (11) (2016) 5161–5173.
[127] M.G. Rosca, et al., Cardiac mitochondria in heart failure: decrease in respirasomes and oxidative phosphorylation, Cardiovasc. Res. 80 (1) (2008) 30–39.